DEVELOPMENT OF REGENERATIVE EXTRACELLULAR VESICLES FOR BONE TISSUE ENGINEERING

UNIVERSITY OF BIRMINGHAM

Dimitra Tsaroucha

A thesis submitted to the University of Birmingham for the degree of Masters by Research Thesis

School of Chemical Engineering

April 2019

Supervisors: Dr. Sophie Constance Cox, Prof. Liam Grover,

Prof. Moataz Attallah,

Dr. Owen Davies (External, Loughborough University)

TABLE OF CONTENTS

LIST OF FIGURES

LIST OF TABLES

ABSTRACT

There are a number of clinical strategies to promote fracture healing and treat bone defects, such as autologous or allogenic bone grafting procedures and stem cell therapies. Stem cell therapies have shown great potential in the area of regenerative medicine and tissue engineering. However, numerous considerable limitations are associated with the presented techniques, including limited supply in donor tissue, often insurmountable regulatory hurdles, ethical and economic issues. Extracellular vesicles (EVs) have gained considerable attention in tissue engineering as a new potential therapy that enables bone and tissue healing. EVs are nano-sized particles that are released into the cellular environment from all types of cells contributing to cell-to-cell communication. Naturally EVs deliver important biological cargo including nucleic acids and osteoinductive proteins. An EV approach to tissue engineering could eliminate the significant issues with grafting procedures and provide an alternative therapy to the current biological therapies. However, the separation and identification of regenerative EV populations is currently problematic due to the variability that exists in vesicles and isolation protocols.

The vast part of this study concerns the isolation and characterisation of osteoblastic EVs. EVs were isolated by two different methods; sequential and differential ultracentrifugation. Their size distribution and morphologies were determined via three different microscopy techniques such as dynamic light scattering (DLS), nanoparticle tracking analysis (NTA) and transmission electron microscopy (TEM). The total protein content was analysed using a protein quantification assay (BCA) and the influences of these EVs on osteoblast metabolism were assessed using an Alamar Blue assay (AB).

Finally, formulation of an injectable biomaterial in an effort to facilitate localised EV delivery to a bone defect was explored. The biomaterial of interest in this study was a natural hydrogel called Gellan Gum (GG). Gellan Gum (GG) is commonly used in the food and pharmaceutical industries as a thickening agent. In this study, different cross-linker solutions were prepared and evaluated as a potential injectable system that may be used to controllably deliver therapeutic doses of isolated vesicles.

In order to produce an injectable gel, toothpaste was considered as a baseline material with desirable rheological characteristics. The rheological behavior of GG sample was tested and compared to that of a toothpaste.

EVs were successfully isolated using both protocols. The highest centrifugal forces; 75,000 x g and 120,000 x g gave the highest concentration of EVs that were capable to enhance cell proliferation in culture. Also, at these two centrifugal forces in both protocols, EVs with similar average sizes appeared. Future work would focus on the incorporation of EVs into optimised GG hydrogels and *in-vitro* testing of mineralisation.

AIM AND OBJECTIVES

The main goal of the present work was to assess and compare the various osteoblastic EVs factions isolated from conditioned culture media (CCM). Two different protocols, consisting of five different centrifugation speeds, were compared with the view of selecting a protocol tailored to osteoblast EVs and consequently contribute to the field's understanding of ultracentrifugation optimisation.

These two protocols, namely sequential and differential, have been compared based on the size, concentration and protein content of isolated EVs in order to identify similarities and differences. Also, in this study design parameters for the development of a physically cross - linked Gellan Gum (GG) hydrogel, as a potential injectable vehicle composited with purified osteogenic EVs to enable localised release was explored.

To achieve the overarching aim of this thesis the following objectives were defined:

Objectives:

- Purify intact EVs using two different methods of isolation; sequential and differential ultracentrifugation.
- Define EV size, morphology and concentration using dynamic light scattering (DLS), nanoparticle tracking analysis (NTA) and transmission electron microscopy (TEM). Following, assess protein content (BCA Assay) of the purified vesicles and their influence on cellular metabolic activity (Alamar Blue Assay) to select an optimum isolation protocol.
- Formulate injectable Gellan Gum hydrogels with comparable rheological behavior to toothpaste for the design of a vesicle injectable system.

CHAPTER 1 – LITERATURE REVIEW

The requirement for effective bone regeneration therapies is huge. Every year more than 1.5 million individuals worldwide undergo graft surgeries to replace or repair bone; lost to disease, genetic abnormalities or trauma (Goldring and Gravallese, 1999; Jahangir *et al*., 2008; Wang and Yeung, 2017; Kowalczewski and Saul, 2018). This has an associated annual cost of more than $2.5 billion and is anticipated that it will increase at a compound annual rate of 7 – 8% (Jahangir *et al*., 2008; Kowalczewski and Saul, 2018).

Several studies reported that 5 – 10% of bone fractures, which occur from trauma, age and chronic diseases such as osteoporosis and rheumatoid arthritis, may heal insufficiently due to limited bone formation (Mathew and Hanson, 2009; Fisher *et al.*, 2016). These defects are usually associated with loss of function and pain, influencing an enormous number of individuals around the world, causing chronic disabilities and in some cases shorter life expectancy. Fracture healing has been promoted through the use of various treatment methods including internal and external fixation and autologous/allogeneic bone grafting (Robert and Rosenbaum, 2012; Bennett *et al.,* 2012; Goodman *et al.,* 2013; Fisher *et al.*, 2016; Qin *et al*., 2016). The aim of these treatments is to provide stability and the return of bone function as quickly and completely as possible.

Autologous bone grafting is a process during which bone or tissue graft is transferred from one body site to another body site in the patient. This particular type of bone grafting is regarded as the “gold” standard for the replacement of bone since it minimises immunological rejection and provides the best osteoinductive properties (Robert and Rosenbaum, 2012; Fisher *et al.*, 2016; Kowalczewski and Saul, 2018). Allogenic grafting refers to tissue or bone that is collected from a donor, in most cases from a human cadaver, and transplanted to a recipient (Robert and Rosenbaum, 2012). Nevertheless, roughly 20 to 30% of patients who undergo autologous bone grafting procedures suffer from donor-site morbidity and 30% of patients who undergo allogenic bone grafting procedures suffer from complications such as infection and fracture, increasing significantly the treatment cost and operative time (Robert and Rosenbaum, 2012; Qin *et al*., 2016; Kowalczewski and Saul, 2018).

In addition, there is a limit to the amount of autologous/allogenic tissue and bone that can be harvested and therefore large defects may not be treatable. In summary, all the above methods are not optimal due to limited availability and high risks of complication (Nandi *et al.*, 2010; Matassi *et al.,* 2011; Qin *et al*., 2016).

In response to these limitations, researchers have focused on the development of regenerative medicine and tissue engineering strategies. These fields aim to repair damaged and diseased tissues or organs using biomaterials and autologous cells. Ceramics, natural and synthetic polymers have been widely investigated as candidate biomaterials for the development of implants to deliver therapeutics that promote bone and tissue repair (Deng *et al*., 2011).

1.1 Regenerative medicine and tissue engineering

Regenerative medicine (RegMed) is a broad area that focuses on the regeneration, replacement and enhanced healing of tissues or organs. These can be achieved by stimulating irreparable organs to restore themselves or even incorporate cells with biodegradable and biocompatible materials to participate in tissue formation (Figure 1) (Polykandriotis *et al.*, 2010; Lamichhane *et al.*, 2014; De Jong *et al*., 2014). RegMed consists of two critical approaches. The first approach is based on cell therapies, in this case the cells have been administered to repair a tissue via paracrine functions or directly (De Jong *et al*., 2014; Mao and Mooney, 2015). The second approach is mention as tissue engineering. This particular approach is based on the integration and incorporation of cells with biocompatible scaffolds to form a tissue (Figure 1) (De Jong *et al*., 2014; Mao and Mooney, 2015). In this case the cells have been expanded in the laboratory under specific conditions and have been seeded onto or in a scaffold made of biocompatible materials that is implanted back to the patient as a therapy (De Jong *et al*., 2014; Mao and Mooney, 2015).

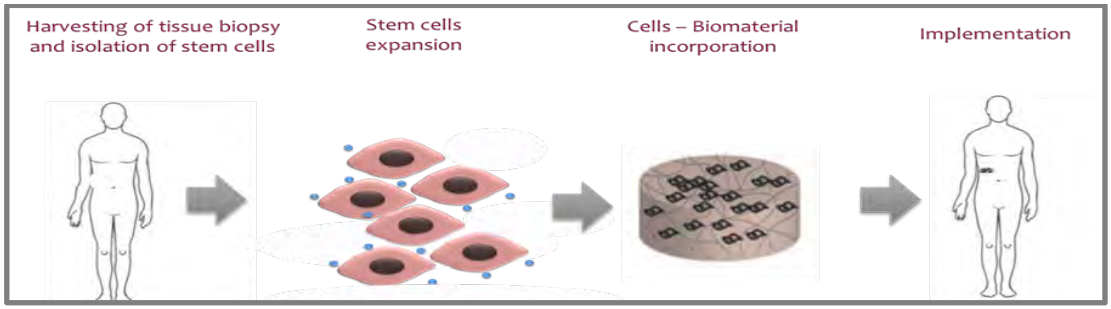

Figure 1. Overview of tissue engineering approach. The incorporation of cells with a biomaterial scaffold. The autologous cells may be collected directly from the patient and are expanded in the laboratory under specific conditions. Next, the cells are seeded onto or in a scaffold in order to be implanted back to the patient as a therapy (Lamichhane et al., 2014; De Jong et al., 2014).

Bone formation, development, repair, and remodelling are continuous processes throughout life. In recent years, stem cell - based approaches have gained considerable attention in tissue engineering since they can be used as an alternative biological method to classic cell therapies.

In the case of orthopaedic injuries, the use of stem cells as a therapy may reduce the pain, increase the functionality and heal stubborn injuries. Several studies have been reported that mesenchymal stem cells (MSCs) derived from bone marrow have the ability to differentiate and inform new tissues in orthopaedics that make up cartilage, tendons, muscles and bones (Centeno *et al*., 2010; Wei *et al*., 2013; Wang *et al*., 2017). Stem cells are unspecialised and undifferentiated cells. A variety of sources are being applied to specialise stem cells or even generate cells with osteoblastic activity. An example is the osteoblastic cells that are derived from osteoprogenitor cells having mesenchymal origin. This particular type of cell is located in bone marrow and is responsible to promote and stimulate bone formation by calcium and phosphate mineralisation (Jayakumar and Di Silvio, 2010; Qin *et al*., 2016).

Osteoblastic cells have been shown to be an essential factor in bone regeneration technologies (Reisman and Adams, 2014; Qin *et al*., 2016). Several studies have demonstrated that stem cells generate and release a broad range of proteins, cytokines and growth factors that are involved in the restoration of damaged tissue (Ong and Wu, 2015).

According to Ong and Wu, recent studies have shown that the physical presence of stem cells is not obligatory and beneficial effects within the infracted heart can be derived just from the administration of cells' conditioned media (CCM) (Ong and Wu, 2015). Vrijen *et al. (*2010) and Lai *et al.* (2015) reported that molecules derived from MSC have functions similar to those of MSC including suppression of inflammatory responses and repair of damaged tissue (Vrijen *et al.,* 2010; Lai *et al.,* 2015). Based on these indications, numerous studies have shown that stem cells are able to release factors such as nanosized heterogeneous membrane vesicles, microvesicles and exosomes, into the cellular environment contributing to cell-to-cell communication (Raposo and Stoorvogel, 2013; Lamichhane *et al.*, 2014; Zaborowski *et al.*, 2015; Bruno *et al.*, 2016; Qin *et al*., 2016; Mendes *et al.,* 2016; Cunnane *et al*., 2018).

The above studies provide novel insights into the potential application of extracellular vesicles as a cell - free therapeutic system to use in place of autologous and allogeneic stem cell administration (Vrijen *et al.,* 2010; Ratajczak *et al.*,2012; Ong and Wu, 2015; Lai *et al*., 2015).

1.2 Introduction to Extracellular Vesicles (EVs)

Translation of stem cell therapies are often prevented by insurmountable regulation, ethical and economic issues. Small soluble molecules including cytokines and growth factors are secreted into the cellular environment from stem cells. Recent studies have shown that nano-sized particles which elicit biological activity are released by stem cells. These particles called extracellular vesicles (EVs) (Vrijen *et al.,* 2010; Yeo *et al.*, 2013; Lai *et al.,* 2015; Azoidis *et al*., 2018).

EVs were first detected by Wolf in the late 1960s. EVs were found within the platelets and described as "platelet dust" (Wolf, 1967; Azoidis *et al*., 2018). In 1967, Bonucci and Anderson, identified small electron – dense particles attached to collagen fibrils in a cartilage matrix. These electron - dense particles were defined as matrix vesicles (MVs) (Bonucci, 1976; Anderson, 1976; Azoidis *et al*., 2018). In 1980, these vesicular particles were shown to participate in immunological procedures (Tram *et al.,* 1981; Ronquist and Brody, 1985; Azoidis *et al*., 2018).

Today, EVs are defined as nano-sized heterogeneous messengers that are released upon fusion with the plasma cell membrane into the cellular environment allowing intercellular communication and enhanced cell differentiation (Figure 2) (Raposo and Stoorvogel, 2013; Lamichhane *et al.*, 2014; Bruno *et al.*, 2016; Qin *et al*., 2016; Mendes *et al.,* 2016; Zaborowski *et al.*, 2015; Cunnane *et al*., 2018; Bebelman *et al.*, 2018).

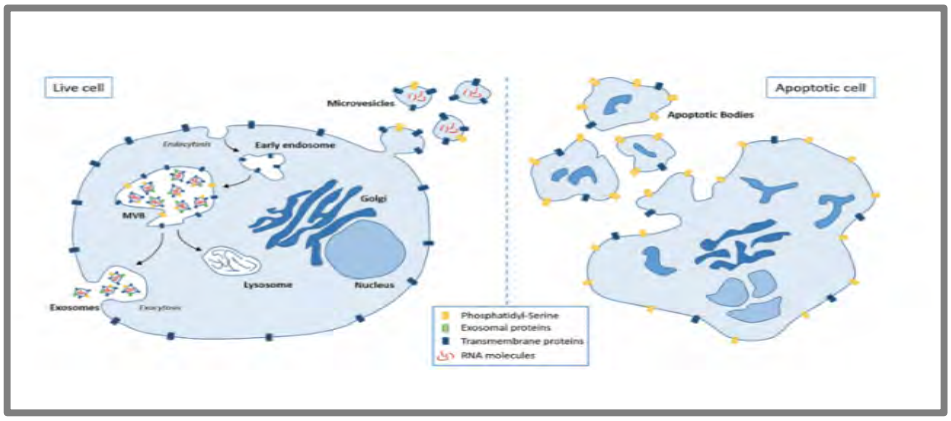

Figure 2. Schematic presentation of intracellular release of EVs (Bruno et al., 2016).

EVs have been detected and isolated from a wide range of biological fluids including lymph, saliva, ascetic fluid, urine, blood, semen, bile and cerebrospinal fluid (Hu *et al*., 2012; Szatanek *et al.*, 2017; Konoshenko *et al*., 2018). Also, EVs can be isolated from cell culture supernatants of several cell types including, mesenchymal stromal (MSC), immune cells (dendritic), bone marrow stem cells (BMSC) and human neural stem cells (hNSCs) (Momen-Heravi *et al.,* 2013; Yuana *et al*., 2013; Lamichhane *et al.*, 2014; Zaborowski *et al*., 2015; Mendes *et al.,* 2016; Azoidis *et al*., 2018). Multiple contents have been reported in isolated vesicle populations including proteins, messenger RNAs (mRNAs), microRNAs (miRNAs) and lipids (Momen-Heravi *et al.,* 2013; Yuana *et al*., 2013; Lamichhane *et al.*, 2014; Zaborowski *et al*., 2015; Mendes *et al.,*2016; Azoidis *et al*., 2018).

EVs can be distinguished into three different types according to their diameter and mechanism of biogenesis such as apoptotic bodies, microvesicles and exosomes (Momen-Heravi *et al.,* 2013; Yuana *et al*., 2013; Lamichhane *et al.*, 2014; Zaborowski *et al*., 2015; Mendes *et al.,*2016; Azoidis *et al*., 2018).

Apoptotic bodies are the larger particles (50 – 4000 nm), which are released upon the fragmentation of plasma membrane by apoptosis having a heterogeneous shape. The protein markers of apoptotic bodies are C3b, TST and histones (Bruno *et al.*, 2016; Willms *et al*., 2016; Ha *et al*., 2016; Szatanek *et al.*, 2017; Konoshenko *et al*., 2018; Azoidis *et al*., 2018; Harjes *et al*., 2019). Microvesicles (50 – 1000 nm) are smaller than apoptotic bodies and larger than exosomes. Microvesicles are produced by direct budding of the plasma membrane having various shapes containing nucleic acids and cytosolic proteins. The protein markers that are presented in the microvesicle population are CD40, integrins and selectins (Mendes *et al.,* 2011; Momen-Heravi *et al.,* 2013; Yuana *et al*., 2013; Lamichhane *et al.*, 2014; Zaborowski *et al*., 2015; Ha *et al*., 2016; Willms *et al*., 2016; Szatanek *et al.*, 2017; Azoidis *et al*., 2018; Konoshenko *et al*., 2018; Harjes *et al*., 2019). Exosomes (20 – 150 nm) are released by the fusion between plasma membrane and multivesicular bodies (MVB), having endosomal origin. Several studies reported that exosomes have a uniform circular shape and contain specific proteins, including heat shock proteins (CCT2, HSPA5, HSP60, HSP70 and HSP90), endosomal trafficking proteins (Alix and TSG101), Flotillin, and tetraspanin proteins (CD9, CD63 and CD81). The membranes of exosomes contain ceramide, sphingomyelin, cholesterol, phosphatidylinositol, lipid rafts which are related to proteins (e.g glycosylphosphatidylinositol), phosphatidylserine and phosphatidylethanolamine (De Jong *et al*., 2014; Zaborowski *et al*., 2015; Bruno *et al.*, 2016; Ha *et al*., 2016; Szatanek *et al.*, 2017; Konoshenko *et al*., 2018; Harjes *et al*., 2019). Remarkably, there is an inconsistency within the literature concerning the size range of each EV subtype.

The natural capability of EVs, both microvesicles and exosomes, to deliver biological cargo has attracted attention since they could be used as a delivery vehicle for osteoinductive proteins and nucleic acids that are highly effective in bone regeneration technologies. Nevertheless, the identification of these specific sub-populations is problematic due to the variability that exists in vesicles sizes, way of formation, shape and source (Lamichhane *et al.*, 2014; Konoshenko *et al*., 2018).

Therefore, in this thesis, the EV population will not be fractioned into exosomes or microvesicles instead the focus is to compare the relative proportion within a mixed sample and assess potential therapeutic efficacy.

1.2.1 Isolation Methods for EVs

EVs can be isolated from cells and biological fluids via several methods including, ultracentrifugation, ultrafiltration, size exclusion chromatography, polymer - based precipitation and immunoaffinity separation (Witwer *et al.*, 2013; Raposo and Stoorvogel, 2013; De Jong *et al*., 2014; Zaborowski *et al*., 2015; Yakimchuk, 2015; Bruno *et al.*, 2016; Konoshenko *et al*., 2018). Differential ultracentrifugation is the most broadly used method for the EVs isolation (Zaborowski *et al*., 2015). However, it should be noted that differential ultracentrifugation, like other existing methods, may not efficiently separate completely microvesicles from exosomes or apoptotic bodies and even protein aggregates. New techniques have also been explored for the extraction of EVs from cells and all the biological fluids, including microfluidic devices, antibody magnetic beads and advanced filtration technologies (Momen-Heravi *et al.,* 2013; Cheung *et al.*, 2018). However, the assessment of EV (microvesicles and exosomes) sizes and concentrations is technically complicated due to the heterogeneity of EVs population and also the wide range of quantitative methods used for the determination of these particular characteristics (Lamichhane *et al.*, 2014; De Jong *et al*., 2014; Zaborowski *et al*., 2015; Konoshenko *et al*., 2018). There is an imperative need for efficient and reliable techniques of vesicles isolation so that all recent studies can be more standardised and efficient.

1.2.1.1 Differential centrifugation and ultracentrifugation

The differential centrifugation method is based on sequential centrifugation steps at different centrifugal forces. This method aims to separate particles according to their buoyant density (Lai *et al*., 2011; Tatischeff *et al*., 2012; Witwer *et al*., 2013; Yakimchuk, 2015; Szatanek *et al*., 2015; Zhou *et al*., 2016). Several protocols involve a few sequential centrifugation speed spins. These centrifugation speeds are reported in both g and rpm within the literature. Typically, the initial centrifugal spin is designed to remove dead cells with centrifugation forces ranging from 300 to 2,000 x g for 10 to 30 minutes (Lai *et al*., 2011; Tatischeff *et al*., 2012; Momen-Heravi *et al.,* 2013; Zaborowski *et al*., 2015; Yakimchuk, 2015; Szatanek *et al*., 2015; Konoshenko *et al*., 2018). Followed by a second spin to remove apoptotic bodies and aggregates of biopolymers with centrifugation forces ranging from 10,000 to 20,000 x g for 20 to 30 minutes (Lai *et al*., 2011; Tatischeff *et al*., 2012; Momen-Heravi *et al.,* 2013; Witwer *et al*., 2013; Zaborowski *et al*., 2015; Yakimchuk, 2015; Szatanek *et al*., 2015; Zhou *et al*., 2016; Konoshenko *et al*., 2018). In the final stage, supernatant from the second spin is subjected to a final round of centrifugation. The centrifugation forces vary at this particular speed from 100,000 to 200,000 x g maintained for 70 to 120 minutes (Lai *et al*., 2011; Tatischeff *et al*., 2012; Momen-Heravi *et al.,* 2013; Witwer *et al*., 2013; Zaborowski *et al*., 2015; Yakimchuk, 2015; Szatanek *et al*., 2015; Zhou *et al*., 2016). The non – vesicle proteins in the vesicle pellet are removed by multiple washings with phosphate buffered saline (PBS) at 100,000 x g for 70 minutes (Lai *et al*., 2011; Momen-Heravi *et al.,* 2013; Witwer *et al*., 2013; Zaborowski *et al*., 2015; Yakimchuk, 2015; Szatanek *et al*., 2015; Zhou *et al*., 2016). However, the multiple washes not only enhance the vesicles' purification but also can decrease their quantity and quality (Livshits *et al*., 2015; Konoshenko *et al*., 2018). An additional disadvantage for this method is that the high ultracentrifugation forces allow the formation of EV aggregates decreasing the efficacy of EVs' isolation (Mol *et al*., 2017; Konoshenko *et al*., 2018). That said, ultracentrifugation allows for relatively rapid processing of large volumes of cell culture medium quantities that may not be possible with other methods (Konoshenko *et al*., 2018; Chen *et al*., 2019).

1.2.1.2 Ultra - Filtration

Ultra - filtration techniques have been used for the collection of microvesicles and exosomes (Yakimchuk, 2015; Konoshenko *et al*., 2018). Filtration membranes with pore diameters of 0.1, 0.22, 0.45 and 0.8 μm are used to "trap" vesicles with diameters larger than 100, 200, 450 and 800 nm. Insoluble molecules and big particles removed first. In particular, filters with pore diameter of 0.45 and 0.8 μm are used to collect particles with diameters larger than 800 nm or 400 nm. In the following step, particles with smaller size than the target of EVs are separated by filters with pore diameter of 0.1 and 0.22 μm (Witwer *et al.*, 2013; Yakimchuk, 2015). Thus, the EV fraction of a specified size is concentrated by the filtration membrane. However, the ultrafiltration method has a significant disadvantage; the additional forces which are applied to pass the liquid of particles via the filtration membrane, could potentially cause damage to the vesicles' surface (Wang *et al.*, 2013; Yakimchuk, 2015; Konoshenko *et al*., 2018).

1.2.1.3 Size exclusion chromatography

Size exclusion chromatography (SEC) is often used to separate large molecules (cells, debris) and small molecules (microvesicles, exosomes) on the basis of their size. Briefly, a mixture of molecules dissolved in liquid is applied to a chromatography column packed with porous polymeric beads containing multiple pores and tunnels. These particular beads used to filter small sample molecules which become temporally trapped within the pores (Figure 3). Smaller sample molecules pass around or are excluded from the beads. The large sample molecules cannot penetrate the pores. Thus, these particular molecules elute first, smaller molecules elute later, while molecules that can access all the pores elute last from the column. This method appears to have a main advantage compared to centrifugation techniques; the isolated EVs are not affected by the higher centrifugal shear forces, which may potentially change the structures of the vesicles and also reduce their quality.

The major disadvantage of this method is that it requires a long running time and multiple biological samples (Szatanek *et al*., 2015; Yakimchuk, 2015; Lozano-Ramos *et al*., 2015).

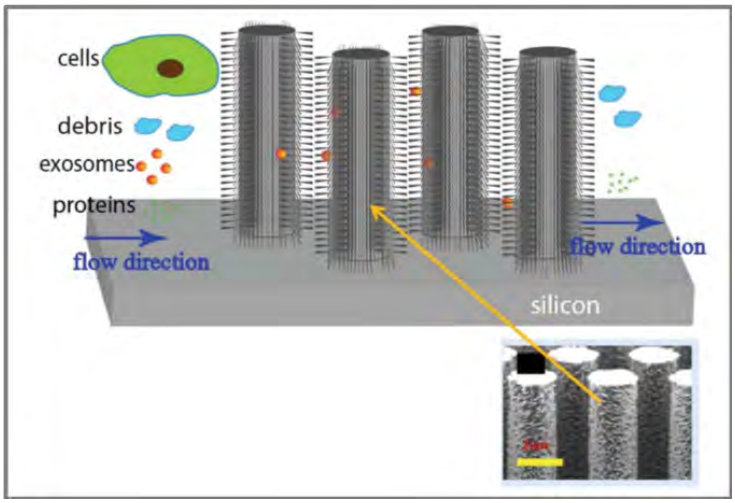

Figure 3. Schematic presentation of ciliated porous structures designed to isolate EVs. These particular structures do not let vesicles larger than 1μm to pass into the wired area while cellular debris, protein and EVs flow through and enter the micropillar area. Cellular debris, protein and EVs are excluded by the nanocilia which from pores with diameter 30 – 200 nm. The ciliated porous structures can then selectively capture microvesicles and exosomes (Wang et al., 2013).

1.2.1.4 Polymer - Based Precipitation

Polymer - based precipitation is used for the isolation of vesicles through a polymer mixing process. This method of isolation usually includes mixing the biological fluid with a polyethylene glycol (PEG) solution and centrifugation at low speed (10,000 x g for 60 mins at 4°C). The polymer precipitation is a quick process that preserves the vesicles' integrity and biological activity. Nevertheless, the presence of the polymeric material may cause contamination to the biological sample and interfere with downstream analysis. The ExoQuick kit (System Biosciences, Mountain View, CA, USA) is frequently used for this method (Yakimchuk, 2015; Szatanek *et al*., 2015; Niu *et al*., 2017).

1.2.1.5 Immunoaffinity separation

This method is based on the vesicles' surface receptors. These particular receptors are used to isolate extracellular vesicles depending on their origin. Briefly, magnetic microbeads coated with an antibody can recognize certain intercellular markers enabling the selection of vesicle population based on the expression of the marker regardless of its size (Figure 4). Intercellular markers that are presented on microvesicle population are CD40, integrins and selectins (Raposo and Stoorvogel, 2013; Bruno *et al.*, 2016; Yakimchuk, 2015; Li *et al*., 2017; Konoshenko *et al*., 2018). Following, the intercellular markers that are contained on the exosome population are tetraspanins family proteins (CD81, CD63 and CD9), heat shock proteins (CCT2, HSPA5, HSP90, HSP70 and HSP60), Alix, Flotillin and TSG101 (Raposo and Stoorvogel, 2013; Yakimchuk, 2015; Bruno *et al.*, 2016; Li *et al*., 2017; Konoshenko *et al*., 2018). This particular technique has the potential for high specificity, an important consideration in the characterisation process of unique vesicle populations (Tauro *et al*., 2012). An important limitation for this method is that the purified EVs can be difficult eluted from the magnetic beads reducing their functional activity and consequently their final concentration (Raposo and Stoorvogel, 2013; Szatanek *et al*., 2015; Yakimchuk, 2015; Bruno *et al.*, 2016; Li *et al*., 2017).

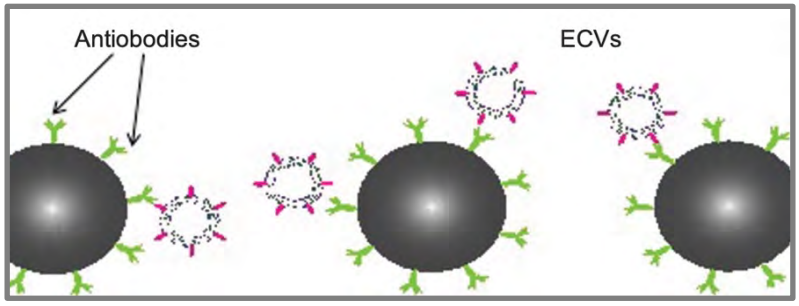

Figure 4. Schematic illustration of antibody coated magnetic beads. This illustration shows how antigens of extracellular vesicles (ECVs) bind to the antibodies of coated magnetic beads (Momen-Heravi et al., 2013).

Method	Time	Advantages	Disadvantages
Differential Centrifugation and Ultracentrifugation	140–600 min	Low cost procedure; isolation from large sample volumes	Damage of EVs; efficiency is affected by the centrifugation forces; only six samples can be concurrently processed in one centrifuge; complexity; low reproducibility
Ultrafiltration	130 min	Simple procedure; no limitations on sample volume	Damage of EVs surface; filter plugging; contamination from proteins; complexity
Size Exclusion Chromatography (SEC)	1mL/min	Reproducibility and purity	Long-time procedure that requires multiple biological samples; specialised equipment
Polymer – Based Precipitation	65 min	Simple procedure; no need in additional equipment	Cost; polymer contamination and retention
Immunoaffinity Separation	65 min	High specificity	Not applicable for large sample volumes; EVs may lose the functional activity

Table 1. A comparison of the most frequently used methods for EVs isolation (Tauro et al., 2012; Wang et al., 2013; Yakimchuk, 2015; Szatanek et al., 2015; Livshits et al., 2015; Lozano-Ramos et al., 2015; Bruno et al., 2016; Li et al., 2017; Niu et al., 2017; Konoshenko et al., 2018; Chen et al., 2019).

1.2.2 Physical analysis of extracellular vesicles (EVs)

Several optical and non - optical techniques have been developed to evaluate EVs based on phenotypical features including size, concentration, density, morphology, charge and mobility (Momen-Heravi *et al.,* 2012; Kooijmans *et al*., 2012; Konoshenko *et al*., 2018). Current available techniques regularly used to characterise EVs, including dynamic light scattering (DLS), nanoparticle tracking analysis (NTA), flow cytometry, western blotting, transmission electron microscopy (TEM), scanning electron microscopy (SEM) and atomic force microscopy (AFM) are summarised in this section with advantages and limitations of each technique highlighted.

1.2.2.1 Optical methods - size, concentration and mobility

1.2.2.1.1 Dynamic light scattering

Dynamic light scattering (DLS) is the most common used optical method to determine the size distribution of nano-sized particles in a solution (Van De Pol *et al*., 2010; Rupert *et al.,* 2017; Hartjes *et al*., 2019). This particular method is based on the analysis of the temporal intensity fluctuations which are caused by Brownian motion of the nanoparticles upon illumination with a laser beam in a solution. Particles undergoing Brownian motion cause intensity fluctuations of scattered light, which is recorded typically in 30 seconds (Figure 5) (Rupert *et al.,* 2017). DLS defines the mobility of the scattering vesicles which are present in the measurement volume. The main advantage of the DLS instrument is the simplicity of typical measurements making it a suitable tool for routine vesicle analysis. The detection limits of DLS ranges from 0.3 nm – 10 µm (Malvern Panalytical, 2019). Thus, small particles can be hidden from the presence of large particles affecting the averaged data and consequently the final results (Van De Pol *et al*., 2010; Rupert *et al.,* 2017).

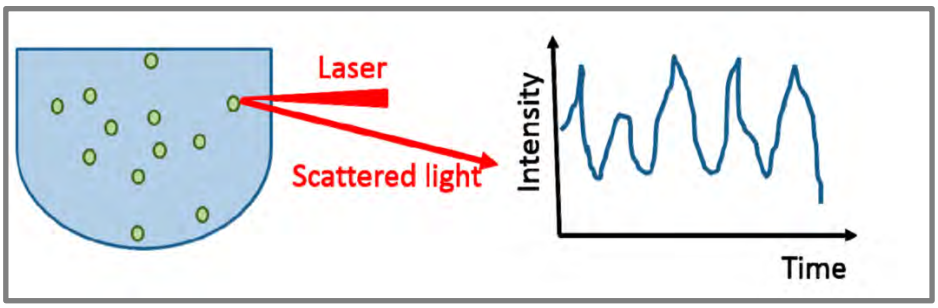

Figure 5. Schematic illustration of a dynamic light analysis (DLS) (Szatanek et al., 2017).

1.2.2.1.2 Nanoparticle tracking analysis

Nanoparticle tracking analysis (NTA) is an alternative method to DLS for evaluating the absolute size distribution and concentration of individual particles. The particles are directly visualised and illuminated by a laser light scattering beam. Their hydrodynamic radius is detected by the principle of Brownian motion (Rupert *et al.,* 2017). A highly sensitive camera records the size and locomotion of the particles (Figure 6). The detection limits of NTA ranges from 10 nm – 2000 nm. In the case of EVs characterisation, NTA instrument has an advantage compared to DLS instrument; its detection limits are lower and close to the sizes of EVs; therefore there is a low possibility to measure large particles and eventually the averaged data in a sample cannot be affected (Malvern Panalytical, 2019). In principle, NTA has to be able to define the size of EVs, however in practice, the analysis seems to be limited by the short-measured trajectories. This is happening due to the diffusion of EVs in and out of the camera focus. Despite this limitation, NTA provides fast assessment and EV size distribution. This method is often used for the antigens detection which are presented on extracellular vesicles by applying fluorescently labelled antibodies. (Van De Pol *et al*., 2010; Momen-Heravi *et al.,* 2012; Witwer *et al.,* 2013; Rupert *et al.,* 2017; Szatanek *et al.*, 2017).

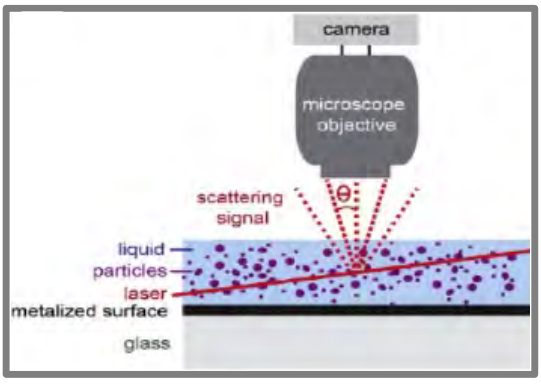

Figure 6. Schematic illustration of a Nanoparticle Tracking Analysis (NTA) instrument by Nanosight (Rupert et al., 2017).

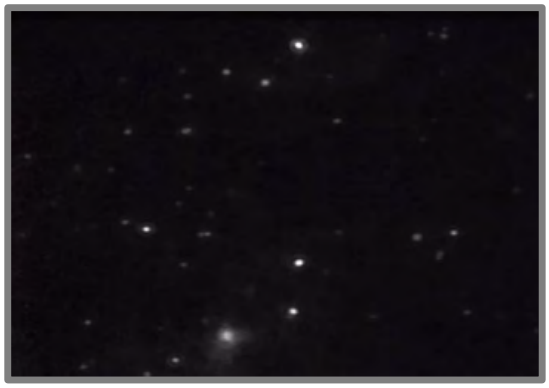

Figure 7. An image of EVs secreted by osteoblasts, cell line MC3T3, acquired by NTA instrument.

1.2.2.1.3 Flow cytometry

Flow cytometry is a powerful technology for scanning and counting single cells with diameter > 1000nm in fluids at a rate of thousands of counts per minute. This method is widely used to record the scattered light and the fluorescence signal, which is generated by single cells using a laser beam as they are passing through a nozzle (Figure 8). In the case of vesicle characterisation, the size can be obtained from the scattering signal. Several authors have suggested that scattering intensity of beads can be used as internal calibration in order to determine the vesicles. However, the accuracy of this particular method is limited because the lower detection limit of flow cytometers for beads is 300 - 500 nm. Thus, only particles with a size higher than 300 nm can be resolved with conventional flow cytometers (Perez-Pujol *et al*., 2007; Robert *et al*., 2009; Van De Pol *et al*., 2010; Momen-Heravi *et al.,* 2012; Witwer *et al.,* 2013).

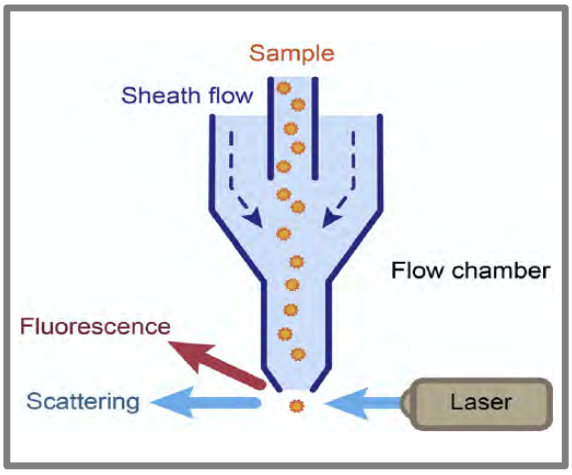

Figure 8. Schematic illustration of a flow cytometer analysis (Rupert et al., 2017).

1.2.2.2 Non-optical methods - Structure and morphology

1.2.2.2.1 Electron microscopy

Transmission electron microscopy (TEM) is the most common surface - based imaging technique, which allows the detection of particles illustrating their structures and morphologies. This particular microscope transmits a beam of electrons via a thin specimen to create an image. Prior to imaging, all the biological samples need to be dehydrated and fixed since TEM is performed most cases under vacuum mode.

A negative staining protocol is also applied in order to enhance the contrast of the imaging. The most commonly used stains are ammonium molybdate, neutral phosphotungstic acid, aurothioglucose and uranyl acetate (UA) (Ohi *et al.*, 2004). On the other hand, scanning electron microscopy (SEM), scans a beam of electrons on a thin sample over the surface and collects the scattered electrons, yielding a topographical image of the surface. (Momen-Heravi *et al.,* 2012; Rupert *et al.,* 2017).

Both of these imaging techniques have an important limitation; sample preparation and imaging conditions may damage fragile vesicles and as such their sizes and morphologies may be altered from their native state if care is not taken (Momen-Heravi *et al.,* 2012; Witwer *et al.,* 2013; Rupert *et al.,* 2017). Notably, TEM has a higher resolving power than SEM, thus cellular structures of the sample can be viewed at very high magnifications. That said, TEM is a readily used method to qualify size distributions obtained from techniques, such as DLS or NTA, while also providing additional information about EV morphology and electron density (Momen-Heravi *et al.,* 2012; Witwer *et al.,* 2013; Rupert *et al.,* 2017). Figure 9 is an example TEM image obtained as part of this thesis and used in a wider study concerning osteogenic EVs (Davies *et al*., 2017). This image was used to qualify vesicle size and demonstrate circular heterogenous morphologies.

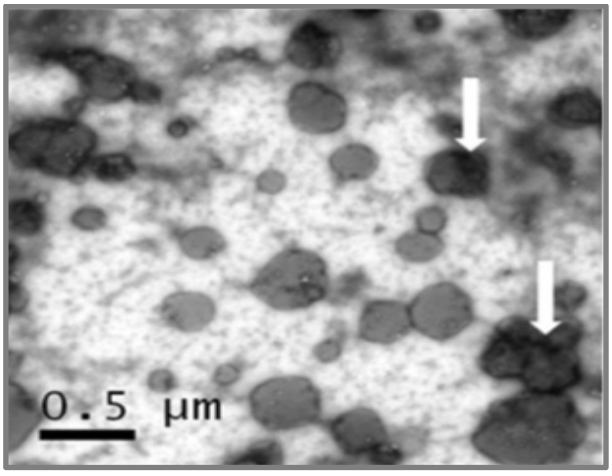

Figure 9. TEM analysis of EVs populations isolated from MC3T3s revealed a heterogeneous population of circular vesicles ranging in size from 20 - 200 nm (Davies et al., 2017).

1.2.2.2.2 Cryo - electron microscopy

Cryo-electron microscopy (cryofixation) is also used for the size detection of particles. This particular technique enables particle analysis at low temperatures (below -100°C) avoiding the effects of chemical fixation, dehydration and water crystallisation. Imaging is performed under vacuum conditions with samples maintained in a frozen state (Momen-Heravi *et al.,* 2012; Witwer *et al.,* 2013; Rupert *et al.,* 2017). In contrast to mentioned methods of characterisation, cryogenic TEM (Cryo-TEM) and cryogenic SEM (Cryo-SEM) allows direct visualisation and investigation of a biological specimen in their native state. Using Cryo-electron microscopy high resolution images and ultra – structure of the vesicle can be obtained. However, as in other electron microscopic methods of characterisation artefacts may occur in cryo-SEM and cryo-TEM techniques. Ice residuals can remain on the sample from the freezing process, which may led to sample contamination. Furthermore, the time period of a specimen viewing in cryo-SEM and cryo-TEM is often limited due to the samples' sensitivity to radiation damages (Kuntsche *et al*., 2011; Momen-Heravi *et al.,* 2012; Witwer *et al.,* 2013; Rupert *et al.,* 2017; Hartjes *et al*., 2019).

1.2.2.2.3 Atomic force microscopy (AFM)

Atomic force microscopy is a surface - based imaging method, which provides a nanometre, or even sub - nanometre, lateral and vertical resolution of topography. AFM employs an incident laser beam which is focused on the back of a cantilever with a very sharp tip that moves up and down (tapping mode) on the surface of a specimen and the deflections of the beam are captured by a photo diode (Figure 10). AFM is used on dry immobilised EV samples allowing the detection of the size and structure. Additionally, AFM offers high resolution images and also provide the mechanical properties of a sample such as stiffness and elasticity. However, there are difficulties associated with using the sharp AFM tip to probe fragile vesicles as this may cause distortion or damage (Van De Pol *et al.*, 2010; Witwer *et al.,* 2013; Rupert *et al.,* 2017; Hartjes *et al*., 2019).

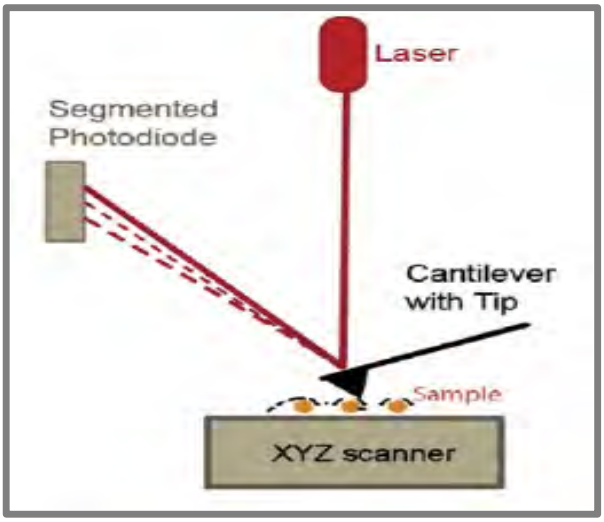

Figure 10. Schematic illustration of an atomic force microscope analysis (Rupert et al., 2017).

Method	Information Acquired	Advantages	Disadvantages
DLS	EVs' size distribution and scattering intensity	Easy and fast procedure	High detection limits; small particles can be hidden from the presence of large particles
NTA	EVs' size distribution and concentration	Low detection limits (10 nm – 2000 nm); low possibility to measure large particles; easy and fast procedure	Limited analysis due to the diffusion of EVs in and out of the camera focus
Flow Cytometry	EVs' absolute number and size	Enables the analysis of thousands of EVs in one sample	Limited accuracy
Electron Microscopy	EVs' size and morphology	Direct visualisation; high resolution images	Damage of EVs surface; sensitivity
Cryo – Electron Microscopy	EVs' size and morphology	Direct visualisation; high resolution images	Sample contamination due to ice residuals; background noise; sensitivity
AFM	EVs' size diameter, three-dimensional topography	High resolution images; mechanical properties of EVs can be obtained	Distortion or damage of EVs surface

Table 2. A comparison of the most frequently used methods for EVs characterisation (Van De Pol et al., 2010; Witwer et al., 2013; Rupert et al., 2017; Szatanek et al., 2017; Hartjes et al., 2019).

1.2.3 Biochemical analysis of extracellular vesicles (EVs)

EVs can be also analysed by their biochemical characteristics (proteins and lipids) (Hartjes *et al*., 2019). Several studies have been reported that proteins and lipids enriched in vesicles populations that are used as detection markers. The protein and lipid content of the vesicles is highly related to the type of cell, biogenesis mode and the lipid content from the surrounding membranes (Rayner and Hannessy, 2013; Vishnubhatla *et al*., 2014; Yanez-Mo *et al*., 2015; Zaborowski *et al*., 2015; Lu *et al*., 2017; Azoidis *et al*., 2018; Thery *et al*., 2018).

In general, according the ExoCarta database, tetraspanins, MHC molecules, fusion proteins (annexins, GTPases), endosomal trafficking proteins (Alix, TSG101) and heat shock proteins (CCT2, HSPA5, HSP60, HSP70 and HSP90) which are involved in multivesicular body of biogenesis, are abundantly detected in vesicles' pellets after their isolation. Tetraspanins (CD9, CD63, and CD81) is a family of transmembrane proteins which recently have been observed in microvesicles. Tetraspanins are mainly involved in cell signalling events and because of their function as mediators are considered to be interesting targets in the area of drug delivery (Raimondo *et al*., 2011; Kooijmans *et al*., 2012; Witwer *et al.,* 2013; Vishnubhalta *et al*., 2014; Yanez-Mo *et al*., 2015; Zaborowski *et al*., 2015; Davies *et al*., 2017; Azoidis *et al*., 2018).

Several lipids are reported to play an essential role in the function of EVs since they bind with proteins and allow the interaction of the vesicle with a cell. The membranes of the vesicles are enriched in cholesterol, prostaglandins (J_2, D_2, E_2 and F_2), sphingomyelin, ganglioside GM3, glycol – sphingolipids, phosphatidylserine and lipoproteins, which are involved in membrane activities including cell attachment and membrane trafficking. Lipoproteins also play an important role in signalling events, since they are comprised of a number of lipids and proteins; which are responsible to deliver cholesterol, fat-soluble vitamins and triacylglycerols to the surrounding tissues. In the profiling of the lipoproteins and lipids content of the vesicles, mass spectrometry, western blotting and liquid chromatography are the most frequently used methods (Raimondo *et al*., 2011; Kooijmans *et al*., 2012; Van Dommelen *et al*., 2012; Witwer *et al.,* 2013; Rayner and Hannessy, 2013; Vishnubhalta *et al*., 2014; Yanez-Mo *et al*., 2015; Zaborowski *et al*., 2015; Azoidis *et al*., 2018).

1.3 Introduction to biomaterials

Bone fracture healing has been promoted through the use of various treatments. Biomaterials are broadly used to restore the function of damaged bone and in some cases to replace it. Biomaterial is any synthetic of natural elements or combination of elements which collaborate with the biological system to replace or treat any organ, tissue or body function (Williams, 1999). Since the environment of the human body is highly chemically and mechanically demanding, the requirements of the candidate materials' properties are quite strict (Navarro *et al.*, 2008).

During the last 60 years, mainly two generations of biomaterials seem to be clearly marked according to their interactions with the host tissues during or after implantation: bioinert (first generation), bioactive and bioresorbable materials (second generation) (Navarro *et al.*, 2008; Cooper, 2015). Bioinert materials constitute the first generation of biomaterials that have limited interaction with the surrounding tissues once implanted in the body. Bioinert materials are used in the field of orthopaedic medicine for the production of fracture plates-screws and implant applications (Navarro *et al.*, 2008; Winkler *et al*., 2018). Some examples of these materials are stainless steel, titanium, zirconia and alumina. Despite their excellent corrosion and mechanical properties, bioinert materials are not biologically recognised by the body (Navarro *et al.*, 2008; Parida *et al*., 2012; Matassi *et al.*, 2013). The second generation of biomaterials arises between 1980 and 2000. Bioactive materials constitute the second generation of biomaterials (Navarro *et al.,* 2008). Bioactive materials are those materials that when implanted can interact with surrounding tissue to enhance biological response. Bioresorbable materials are those materials that when placed in human body start to dissolve and be replaced with advancing tissue (Navarro *et al.,* 2008). The most common bioactive – bioresorbable materials are natural and synthetic origin polymers such as polydioxanone (PDS), poly(3-caprolactone) (PCL), chitosan, poly(2-hydroxyethyl-methacrylate) (PHEMA), polyorthoester, polylactide (PLA), polyhydroxybutyrate (PHB), polyglycolide (PGA) and bio-glasses (Navarro *et al.*, 2008). Polymers have been utilized for a considerable length of time rather than glass and metals in numerous applications because of their great physiochemical properties and their low cost compared to other materials (Chamy and Rosenkranz, 2013).

The third generation of biomaterials are intended to be new biomaterials in order to stimulate particular cellular reactions. These biomaterials properties ought to combine with their capability to signal and trigger particular cellular action and behavior (Navarro *et al.*, 2008).

In recent years, ceramics and biocompatible polymers have been broadly investigated as candidate bio-materials for the development of natural or synthetic bone scaffolds. Advantageously therapeutic molecules may be embedded into these biomaterials to promote bone repair, including extracellular matrix molecules (ECM) such as collagen, vitronectin, laminin, osteopontin, fibronectin and morphogenetic proteins (protein2 - BMP2 and protein7 - BMP7) (Zhang *et al*., 2014; Perez *et al*., 2015; Kowalczewski and Saul, 2018). These particular molecules are an essential factor in bone repair since they have the ability to produce inflammatory molecules essential to stimulate angiogenesis and cell-homing, and consequently contribute to the bone healing process (Zhang *et al*., 2014; Perez *et al*., 2015; Kowalczewski and Saul, 2018).

The procedure of bone repair can be achieved under specific conditions, meaning the presence of cells which is capable to restore the damaged structure and a micro-environment may support regeneration. Introduction of porosity into bone scaffolds has been widely explored. Physically this network may provide the appropriate micro-environment for cell retention and support infiltration of vasculature and nutrients into the structure. Scaffolds and implants can either be of natural origin (natural hydrogels) or synthetic biomaterials including synthetic polymers and ceramics (De Jong *et al*., 2014).

The last few years, scientists have focused on the construction of biomimetic and bio-inspired materials such as natural and synthetic derived polymers, which can be easily incorporated with the body functions, integrate with extracellular matrix components and regenerate bones and tissues. Bio-inspired materials also referred to as biomimetic; is any synthetic or natural element, or combination, whose structure and functions mimic those of the native tissue. The main purpose of this type of biomaterial is to collaborate with the biological system and treat or replace any function.

The requirements of the candidate bio-materials properties are quite strict due to the physiological environment within the body, which is chemically and mechanically demanding. Thus, materials with high molecular properties such as natural or synthetic derived polymers need to be investigated (Meyers *et al*., 2008; Stevens, 2008; Navarro *et al.*, 2008; Williams, 2008; Cooper, 2015). Natural and synthetic derived polymers which are used in bone repair technologies, such as chitosan, alginate, hyaluronic acid (HA), Collagen (Type-I), silk fibroin and gellan gum (GG) are presented in this section of the report.

1.3.1 Injectable hydrogels

A variety of hydrogels are used in tissue engineering as a "system of support" that provides the appropriate micro - environment for cell maintenance, retention and immobilisation (Figure 11). Hydrogels are usually descripted as three - dimensional, hydrophilic networks having the capability to absorb large amounts of biological fluids and water. Hydrogels are classified by their origin in two categories, natural or synthetic (Drury and Mooney, 2003; Lanza *et al*., 2014; Sheikh *et al.,* 2015; Radhakrishnan *et al*., 2016).

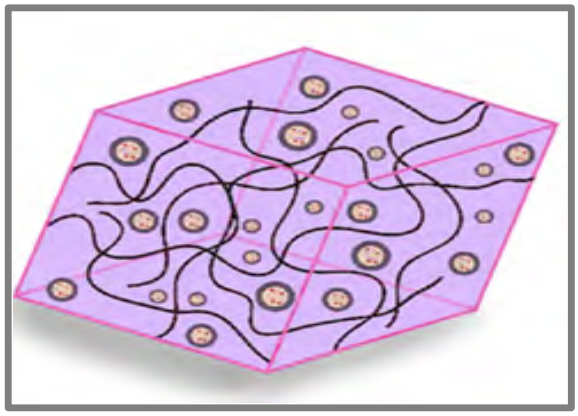

Figure 11. Schematic presentation of a cell-material microenvironment (Lamichhane et al., 2014).

Recently, a range of natural hydrogels have gained considerable attention, in both areas of bioengineering and drug delivery, due to their desirable properties including processability, tailored chemistry, biocompatibility, biodegradability and high - water content (Drury and Mooney, 2003; Lanza *et al*., 2014; Sheikh *et al.,* 2015; Kowalczewski and Saul, 2018; Radhakrishnan *et al*., 2016).

Natural hydrogels including Collagen (Type-I), Silk fibroin, Chitosan, Alginate and Gellan gum, are widely used for the construction of natural biocompatible implants and scaffolds for wound healing, bone regeneration and drug delivery systems (Drury and Mooney, 2003; Sheikh *et al.,* 2015; Lanza *et al*., 2014; Radhakrishnan *et al*., 2016; Kowalczewski and Saul, 2018).

In the field of drug delivery, injectable hydrogels used as a delivery vehicle capable of locally releasing a therapeutic molecule, minimises surgical procedures, and invasiveness for the patient (Kretlow *et al*., 2007). Of these natural hydrogels, gellan gum gels, have received a great attention due to their well - documented physical properties such as low toxicity and high biocompatibility. The above characteristics have made gellan gum a suitable material for the delivery of therapeutic molecules such as EVs (Lanza *et al*., 2014; Radhakrishnan *et al*., 2016; Kowalczewski and Saul, 2018).

1.3.1.1 Synthetic Hydrogels

Synthetic hydrogels have a high - water absorption capacity and strong chemical performance providing a long service life to a patient. Synthetic hydrophilic gels such as Polyanhydrides, Polydimethylsiloxane (PDMS), Polyacrylamide (PAM), Polyvinyl alcohol (PVA,) Polylactide acid (PLA), Polyethylene glycol (PEG), Polyethylene oxide (PEO) and polyphosphates can be prepared by different techniques including polymerisation and cross-linking of multifunctional monomers. Their properties can be engineered for chemical and mechanical stability, biocompatibility and several other requirements, such as uniform cell distribution and immobilization. However, the last two decades, scientists have focused on natural origin hydrogels due to their biodegradable and hydrophilic properties (Drury and Mooney, 2003; Goodman *et al.,* 2013; Ahmed, 2015, Sheikh *et al.,* 2015; Tozzi *et al.,* 2016; Tsou *et al*., 2016).

1.3.1.2 Natural derived hydrogels

Interest in natural hydrogels has been increasing due to their desirable molecular properties such as low cytotoxicity, low immunogenicity, high biocompatibility and high degradability.

The natural hydrogels originally can be made from polysaccharides and proteins which are extracted from plants, humans or animals (Drury and Mooney, 2003; Lanza *et al*., 2014; Sheikh *et al.,* 2015; Radhakrishnan *et al*., 2016; Kowalczewski and Saul, 2018).

In this section of the report, the most frequently used natural bio-polymers for bone and tissue engineering such as Chitosan, Gelatin, Alginate, Hyaluronic acid (HA), Gellan gum and proteins (collage Type-l, silk fibroin) will be discussed (De Witte *et al*., 2018). It has to be noted that the above polysaccharide hydrogels can be prepared by different techniques including polymerisation and cross-linking of multifunctional monomer (Drury and Mooney, 2003; Sheikh *et al.,* 2015).

1.3.1.2.1 Chitosan

Chitosan is a linear polysaccharide derived from chitin that can be found in shrimps, fungi, mushroom, lobster, crab and coral (Drury and Mooney, 2003; Venkatesan and Kim, 2010; Radhakrishnan *et al*., 2016). Chitin is one of the most abundant bio – polymer with the highest rate of degradation and production. This type of polysaccharide is composed of (1 → 4) linked N-acetyl-D-glucosamine and N-D-glucosamine groups (Figure 12). The physical properties of the Chitosan, such as biodegradability, non-toxicity, processability, biocompatibility and antibacterial behavior, set it the most broadly used natural polymer for the production of bone scaffolds in tissue engineering (Drury and Mooney, 2003; Radhakrishnan *et al*., 2016; Tsou *et al*., 2016; Kowalczewski and Saul, 2018; De Witte *et al*., 2018).

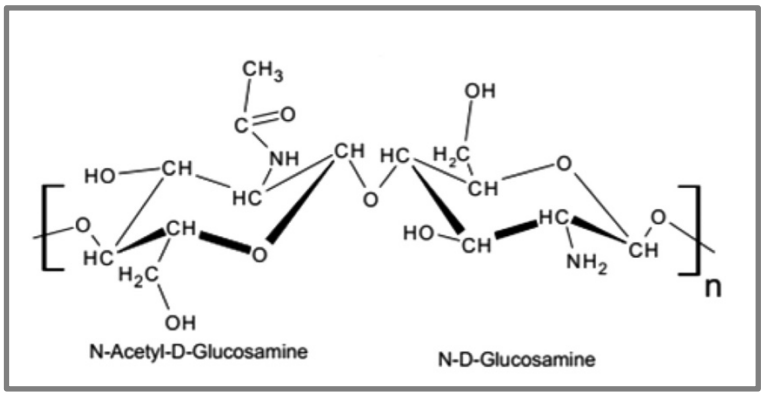

Figure 12. Chemical structure of Chitosan (Radhakrishnan et al., 2016).

1.3.1.2.2 Collagen (Type - I)

Collagen (Type - I) is one of the most important bio – polymers derived from the skins of vertebrate species. Collagen consists of three polypeptide chains which intertwine together into a triple helix structure. Collagen (Type – I) is an attractive biomaterial in bone tissue engineering since is the most abundant protein in bone and tissues (Drury and Mooney, 2003; Sheikh *et al.,* 2015). Collagen play an important role in the promotion of osteogenic differentiation of bone cells through α - β integrin receptor interactions. These particular interactions promote the cell adhesion and consequently cell proliferation. This specific ability of collagen makes it suitable for implants coating and scaffolds production. Also, it may be modified with nanofiber-based growth factors which include bone morphogenetic protein (BMP), vascular endothelial growth factor (VEGF), platelet-derived growth factor (PDGF), transforming growth factor beta (TGF-β) and fibroblast growth factor (FGF) to promote osteogenic differentiation (Drury and Mooney, 2003; Sheikh *et al.,* 2015; Duconseille *et al*., 2015; Tsou *et al*., 2016; Dong and Lv, 2016; De Witte *et al*., 2018).

1.3.1.2.3 Gelatin

Gelatin is a heterogeneous mixture of single or multi stranded polypeptides, each with extended left handed proline helix conformations containing between 50 - 1000 amino acids (Chaplin, 2018). Its amino acid composition is close to that of collagen (Type – I). Gelatin can be extracted from the skin or bones of animals (pigs), insects and fishes by the hydrolysis of collagen and composed of many glycine residues (1 in 3 residues which are arranged every third residue), proline and 4-hydroxyproline residues (Figure 13). Gelatin is used in pharmaceuticals industries for the production of hard or soft capsules, absorbent pad and sealants for vascular prostheses. Its low cost of production, good biocompatibility and non-immunogenic properties are attractive in the field of tissue engineering (Pulat and Akalin, 2013; Hoque *et al*., 2015; Tsou *et al*., 2016; Wang *et al*., 2017; Deshmukh *et al*., 2017).

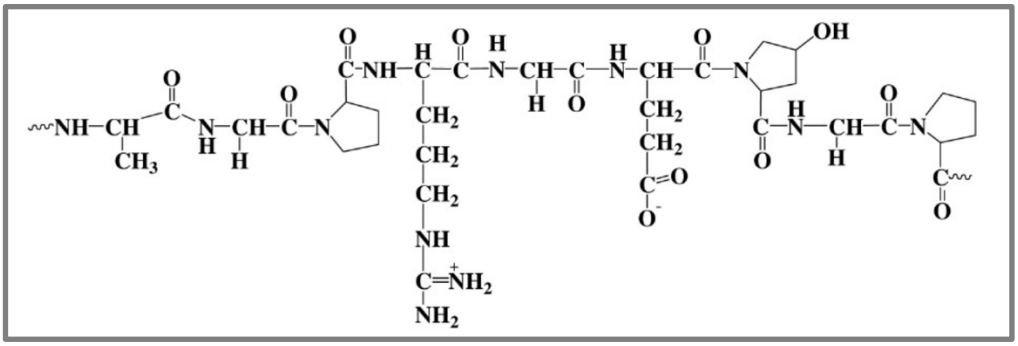

Figure 13. Chemical structure of Gelatin (Deshmukh et al., 2017)

1.3.1.2.4 Alginate

Alginate is a block polysaccharide naturally secreted from bacteria and brown seaweeds. This type of polysaccharide is characterised by an anionic behavior and is composed of β-D-mannuronic acid and α-L-guluronic acid groups linked by (1 → 4) glycosidic linkages (Figure 14) (Zhang *et al*., 2013). Alginate has a unique characteristic; can interact with divalent ions and create a three-dimensional dense structure which called "egg box" improving the mechanical properties. Like chitosan, alginate is characterised by a high biocompatible and degradable polymeric material with low cytotoxicity and cost of production. Among the natural polymers, alginate and chitosan are the most frequently used for bone tissue scaffolding application. However, alginate is also suitable for cell encapsulation techniques such as the allogenic cell implementation for the insulin production for diabetes Type I (Muzzarelli, 2011; Lee and Mooney, 2012; Venkatesan *et al*., 2015; Tsou *et al*., 2016; Radhakrishnan *et al*., 2016; Kowalczewski and Saul, 2018).

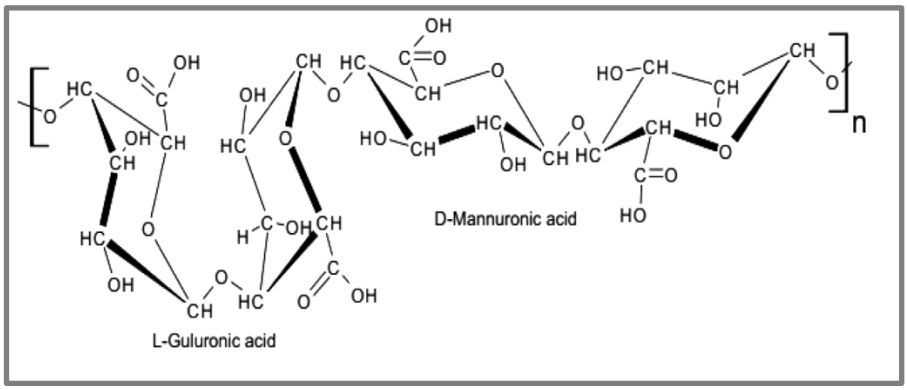

Figure 14. Chemical structure of Alginate (Radhkrishnan et al., 2016).

1.3.1.2.5 Hyaluronic acid (HA)

Hyaluronic acid (HA) is also a linear polysaccharide and released through the body in synovial fluid of joints, extracellular matrix of cartilage and organs during the wound healing process. HA plays also an important role in morphogenesis, angiogenesis and cell signalling phases. This type of polysaccharide consists of β-D-glucuronic acid and N-acetyl-β-glucosamine residues linked by (1 → 3) and (1 → 4) glucoside groups (Figure 15) (Magnani *et al*., 1998). Its high - water adsorption capability and biodegradable properties are extremely attractive in bone repair technologies. Space filling and wound healing scaffolds can be produced from hyaluronic acid enhancing the capability for cell adhesion and differentiation. In the case of bone repair, scaffolds and injectable systems have been recently produced from hyaluronic acid to promote bone healing (Drury and Mooney, 2003; Collins and Birkinshaw, 2013; Sheikh *et al.,* 2015; Tsou *et al*., 2016; Radhakrishnan *et al*., 2016).

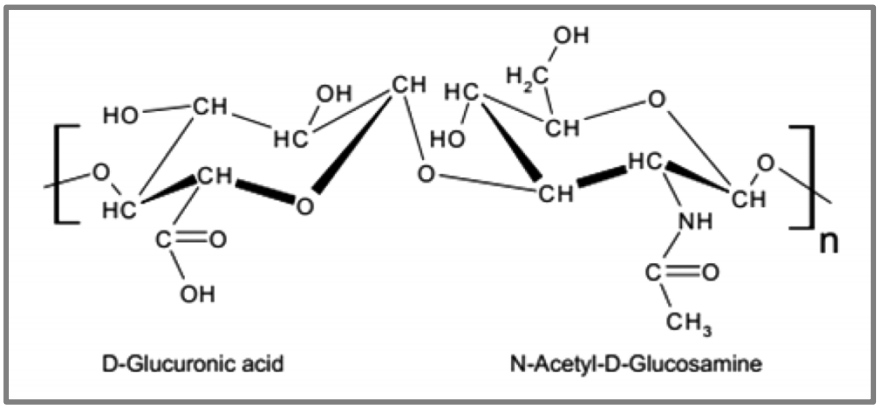

Figure 15. Chemical structure of Hyaluronic Acid (Radhkrishnan et al., 2016).

1.3.1.2.5 Silk fibroin

Silk fibroin (SF) is commonly defined as a natural protein polymer derived from silkworms (*Bombyx mori*), bees and spiders. According to Qi *et al*. (2018), silk fibroin is an attractive biomaterial in bone technology due to its excellent mechanical and biocompatible properties. The silk fibroin consists of two main structural proteins; the heavy chain and the light chain associated through a disulfide bond (Figure 16). The higher molecular weight heavy chain is dominated by the existence of β-sheet. This particular chain is characterised by the presence of 45.9% Gly-cine (G), 30.3% Alanine (A), 12.1% Serine (S), 5.3% Tyrosine, 1.8%Valine and 0.25% Tryptophan (Figure 16). Several studies reported that, biomimetic scaffolds produced from silk fibroin enable the protein bioactivity to be preserved and to enhance osteogenic differentiation (Schlotzer-Schrehardt *et al*., 2013; Qi *et al*., 2017; De Witte *et al*., 2018; Prasad and Mandal, 2018).

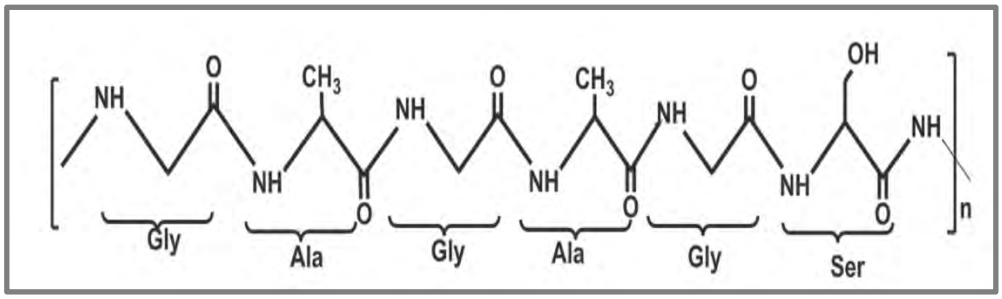

Figure 16. Chemical structure of Silk Fibroin (Prasad and Mandal, 2018).

1.3.1.2.6 Gellan Gum Hydrogel

The biomaterial of interest in this study is a natural hydrogel called Gellan Gum (GG) which is commonly used in the food and pharmaceuticals industries as a viscosity modifier. Gellan gum (GG) is a natural anionic polysaccharide, similar to alginate in utility profile, derived from *Sphingomonas elodea* bacteria (ATCC 31461) by aerobic fermentation. GG is composed of tetrasaccharide (1, 3-b-D-glucose, 1, 4-b-D-glucuronic acid, 1, 4-b-D-glucose, 1, 4-a-L-rhamnose) repeating units and contains one carboxyl side bond (Figure 17). Gellan gum can be formed into gels using either temperature setting or chemical cross-linking using cations. GG is in a coil from at high temperatures. Upon the temperature decrease this coil form is transited to double helix. This particular thermally reversible performance is prerequisite for the gel formation (Nitta and Nishinari, 2005; Sworn, G., 2009; Oliveira *et al*., 2010; Radhakrishnan *et al*., 2016).

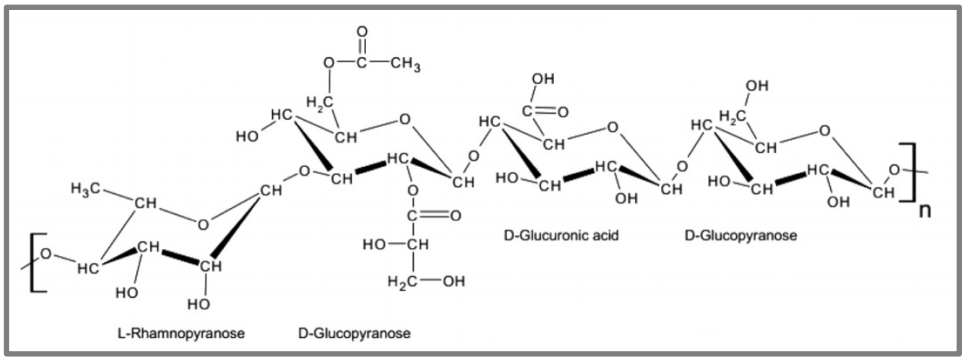

Figure 17. Chemical structure of Gellan Gum (Radhkrishnan et al., 2016).

The physical properties of the GG, such as resistance to heat, high porosity (>90%), non- cytotoxicity, versatility, injectability and physical gelation, make this anionic polysaccharide suitable for therapeutic delivery applications. GG gels have been used in tissue engineering for scaffold production and cell encapsulation providing a specialized environment for isolated cells (Nitta and Nishinari, 2005; Sworn, G., 2009; Oliveira *et al*., 2010; Radhakrishnan *et al*., 2016). However, Gellan Gum is still relatively unknown in the area of biomedical engineering. Only a few studies have searched this material for bone-tissue regeneration and therapeutic delivery applications (Lanza *et al*., 2014; Radhakrishnan *et al*., 2016).

We are proposing to use this biomaterial, GG, in this study to be used in bone or tissue regeneration technologies and therapeutic delivery applications.

One of the most interesting features about Gellan Gum hydrogels is their physical property to remain in gel structure at high temperatures (e.g 37°C) constituting an important factor for the preparation of a stable gel once injected into the human body. Also, its swelling and high porosity properties indicates that this particular polysaccharide may have an appropriate network structure to enable release of incorporated EVs. Thus, controlling GG properties can be beneficial to synthesise a delivery platform for controlled vesicle delivery. One extra parameter for the optimisation of the vesicles release is to incorporate EVs with other molecules (miRNA, collagen and calcium phosphate) once seeded into the GG gels enhancing the osteogenic activity of the vesicles.

1.4 Synthesis of Literature Review

The natural capability of extracellular vesicles (EVs) to mediate therapeutic effects and deliver biological cargo (DNA, mRNA and proteins) makes them an exciting tool for regenerative medicine. There is potential to harness the therapeutic potential of EVs and use biomaterials to locally deliver them to the site of interest (Lamichhane *et al*., 2014). The selection of a suitable bio-material to interact with the vesicles plays an important role to this particular therapeutic approach. This study aims to prepare and define the design parameters for the development of a physically cross – linked Gellan Gum (GG) hydrogels, as a potential injectable gel (vehicle) loaded with purified EVs, enable to maintain them and enhance bone or tissue repair.

CHAPTER 2 – MATERIALS AND METHODS

The present section of the report covers in detail, all the materials and methods used for the isolation and characterisation of EVs as well as the preparation and characterisation of gellan gum hydrogels, including specific techniques and equipment.

2.1 Cell cultures and sample preparation

Murine pre – osteoblastic cells (MC3T3) from a passage 10 were seeded and cultured, at a density of 1 x 10^6 cells/flask, in a T175 flask in minimal essential medium (α – MEM; Sigma – Aldrich, UK) supplemented with 10% (50mL) foetal bovine serum (FBS; Sigma – Aldrich, UK), 2.4% (12mL) L – glutamine (Sigma – Aldrich, UK) and 1% (5mL) penicillin (Sigma – Aldrich, UK), that was replaced every two days. Cells were passaged at a ratio of 1:3 on average every three to four days when they reached 80% confluence according to the standard techniques. All cultures were incubated at 37°C in 5% CO_2.

2.1.1 Osteogenic differentiation

To induce osteogenic differentiation, MC3T3 cells (P15), were cultured in a T175 flask in growth medium (α-minimal essential medium) supplemented with 10% (50mL) foetal bovine serum (FBS; sigma), 2.4% (12mL) L-glutamine and 1% (5mL) penicillin for five days. Next, the α-MEM supplement was replaced by an osteogenic medium. The osteogenic media was consisting of 50 mL exosome depleted growth medium with 10nM sodium β-glycerophosphate and 50μg/mL L-ascorbic acid. For the preparation of osteogenic media, exosome depleted FBS was prepared by the serum ultracentrifugation at 120,000 x g for 16 hours. The cells were cultured in osteogenic medium for a period of 14 days which was replaced every three days. Next the culture conditioned medium (CCM) was collected into 50 mL centrifuge tubes and stored in a fridge for 2 days at 15°C before isolation. All cultures were incubated at 37°C in 5% CO_2.

2.2 Isolation of EVs

2.2.1 Sequential method for EVs ultracentrifugation isolation

EVs were isolated from culture conditioned media (CCM) pooled over the two-week osteogenic culture period. Two different protocols have been used (sequential and differential protocol) and five different speeds (10,000 x g, 20,000 x g, 50,000 x g, 75,000 x g and 120,000 x g) have been applied with the view of selecting a protocol tailored to a specific population.

The sequential method of EVs' isolation consists of five consecutive ultracentrifugation speeds at 10,000 x g, 20,000 x g, 50,000 x g, 75,000 x g and 120,000 x g (Figure 18). Initially, the osteogenic media was centrifuged at 2,000 x g for 20 minutes, in a Mistral 2000 (MSE) centrifuge, to remove the dead cells and the pellet discarded. Afterwards, 19 mL of the supernatant were collected and centrifuged consecutively in an Avanti J-E fixed angle rotor (Beckman Coulter, USA) centrifuge at 10,000 x g, 20,000 x g and then 50,000 x g for 30 minutes respectively. The resulting pellets from each speed were re-suspended in 200µL of PBS and stored at -80°C for further analysis. The collected supernatant was further centrifuged at 75,000 x g in a Sorvall MX 150 Plus (ThermoFisher Scientific, USA) ultracentrifuge for a further 70 minutes. The resulting pellet was re-suspended in 200µL of PBS and stored at -80°C for further analysis. The same supernatant was collected and centrifuged again for the last speed at 120,000 x g for 70 minutes in Sorvall MX 150 Plus (ThermoFisher Scientific, USA) ultracentrifuge to concentrate the pellet of purified EVs. The resulting pellet was re-suspended in 200µL of PBS and stored at -80°C for further analysis. All ultracentrifugation speeds were performed at 4°C.

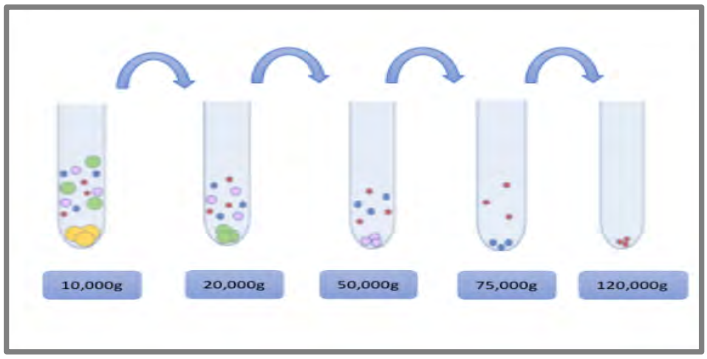

Figure 18. Sequential protocol. Schematic presentation of the sequential isolation of EVs.

2.2.2 Differential method for EVs ultracentrifugation isolation

The differential method of EVs' isolation consists of five individual ultracentrifugation speeds at 10,000 x g, 20,000 x g, 50,000 x g, 75,000 x g and 120,000 x g (Figure 19). The same five speeds were used in both protocols to enable the comparison of isolated EVs' population. Five tubes containing 20 mL of osteogenic media each, were centrifuged at 2,000 x g for 20 minutes each in a Mistral 2000 (MSE) centrifuge and the pellet discarded. Afterwards, 19 mL of each supernatant placed into 20mL tubes and centrifuged individually. Three tubes were centrifuged using an Avanti J-E fixed angle rotor (Beckman Coulter, USA) for 30 minutes each at either 10,000 x g, 20,000 x g or 50,000 x g. All supernatants were removed, and the resulting pellets were re-suspended in 200µL of PBS and stored at -80°C for further analysis. The two remaining tubes were centrifuged in a Sorvall MX 150 Plus (ThermoFisher Scientific, USA) ultracentrifuge at 75,000 x g or 120,000 x g for 70 minutes. The purified EVs' pellets were re-suspended in 200µL of PBS and stored at -80°C for further analysis. All ultracentrifugation speeds were performed at 4°C.

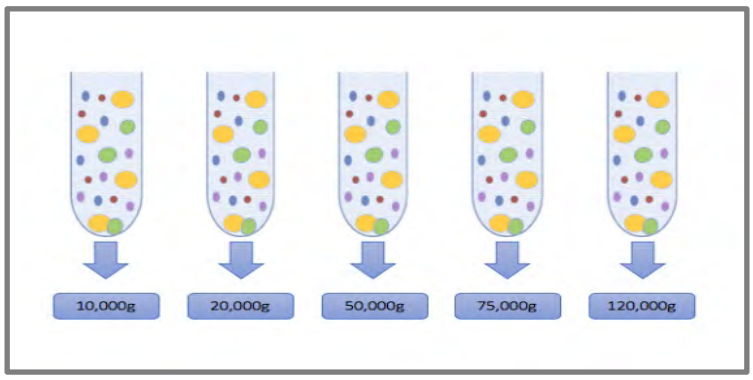

Figure 19. Differential protocol. Schematic presentation of the differential isolation of EVs.

2.3 EVs characterisation

The size distribution and concentration of EVs were obtained for all the speeds (10,000 x g, 20,000 x g, 50,000 x g, 75,000 x g and 120,000 x g) in both protocols (sequential and differential) by dynamic light scattering (DLS) and nanoparticle tracking analysis (NTA). Next, the morphology of isolated EVs by the last two speeds in both protocols, at 75,000 x g and 120,000 x g, was illustrated using transmission electron microscopy (TEM). The protein content of isolated EVs was evaluated for all the speeds in both protocols using a BCA assay. In conclusion, the influence of purified EVs on cellular metabolic activity isolated by the last two speeds in both protocols, at 75,000 x g and 120,000 x g was evaluated by an Alamar Blue Assay (AB).

2.3.1 Dynamic light scattering (DLS)

DLS analysis was performed with a Zetasizer nano - series instrument (Malvern Nano - Zetasizer, = 10 µm laser wavelength), to determine the size distribution of isolated EVs (Apolinário *et al*., 2018). Initially, 20 µL of each sample was dispersed in 700 µL PBS and placed into a cuvette. Prior to DLS analysis, to avoid EVs aggregations all the samples were placed into a sonic bath for 10 minutes. Each sample was analysed five times (n=5) by DLS instrument at 25°C using the Malvern software.

2.3.2 Nanoparticle tracking analysis (NTA)

NTA is the most common instrument for the analysis of EV size distribution and concentration. A NanoSight LM 10 (Malvern Instruments Ltd, UK) microscope equipped with a 455nm laser wavelength, used to determine the size distributions and concentrations of isolated EVs. Initially, 20 µL of each sample was diluted in fresh 700 µL PBS and injected to the laser beam manually. Each sample was analysed five times (n=5) by NTA instrument using NTA 3.2 software. EVs acquisition and videos of 30s were captured at 22°C for each sample.

2.3.3 Transmission electron microscopy (TEM)

A suspension of EVs emerged from the last two speeds at 75,000 x g and 120,000 x g, were visualised using transmission electron microscopy (TEM). Briefly, 20µL of EVs suspension was placed onto a carbon coated film grid (S160-4H Agar Scientific, UK) and allowed to dry for 1 minute at 25°C (room temperature). The excess PBS suspension was gently removed by touching the grid to a tissue paper. Negative staining process was conducted to enhance sample contrast. A single drop (20µL) of 2 % (w/v) uranyl acetate solution (UA) was placed onto the carbon coated film grid and allowed to dry for a period of 1 minute at 25°C (room temperature). The excess UA suspension was gently removed by touching the grid to a tissue paper and the sample was dried for permanent preservation. A JEM 3200FX transmission electron microscope (Joel, USA) was used to image vesicles samples at a voltage of 80 kV.

2.3.4 Bicinchoninic acid assay (BCA)

The detection and quantitation of total vesicle protein contents was assessed with a Thermo Scientific pierce BCA protein assay for all the spins in both protocols. Prior to experiment the preparation of working reagent was necessary. Working agent consists of 1000µL BCA reagent A and 20µL BCA reagent B (plate protocol described in the Pierce instruction booklet). Following, 175µL of working reagent pipetted into a 48 well plate and mixed with 20µL of EVs. The plate was incubated for 30 minutes at 37°C in 5% CO_2. As a positive control, MC3T3s were cultured in growth medium in the absence of EVs. MC3T3 cells from a passage 10 were seeded and cultured, at a density of 1 x 10^6 cells/flask, in a T175 flask in minimal essential medium (α – MEM; Sigma – Aldrich, UK) supplemented with 10% (50mL) foetal bovine serum (FBS; Sigma – Aldrich, UK), 2.4% (12mL) L – glutamine (Sigma – Aldrich, UK) and 1% (5mL) penicillin (Sigma – Aldrich, UK) for three days to reach 80% confluence. The conditioned medium was removed from the flask and 4mL of phosphate buffered saline (PBS) was added to remove CCM residues. Next, the PBS was removed and 4mL of Trypsin (Sigma – Aldrich, UK) was added to the flask. The flask was placed in the incubator for 10 minutes at 37°C in 5% CO_2 to allow cell detachment from the flask bottom.

Afterwards, 4mL of fresh growth medium was added to the cell-PBS suspension and collected to a 50 mL tube which was centrifuged for 3 minutes at 1000 rpm in a Mistral 2000 (MSE) centrifuge. The supernatant was removed and the pellet of the cells was suspended in 1mL of fresh growth medium. Next, the cells were counted with a Neubeuer hemacytometer (Marienfeld) and brought to a concentration of 1 × 10^6 cells/mL. Following, 175µL of working agent pipetted into a 48 well plate and mixed with 20µL of MC3T3s suspension. The plate was incubated for 30 minutes at 37°C in 5% CO_2. The absorbances were measured at 525 nm using the microplate spectrophotometer system (Spectra Max-L-Lumi microplate reader). Each sample was analysed five times (n=5) by the Soft max pro software.

2.3.5 Alamar Blue assay (AB)

Alamar Blue (Sigma-Aldrich) assay kit was used to assess the effect of purified EV dosing on cell metabolic activity. MC3T3 cells from a passage 10 were seeded and cultured, at a density of 1 x 10^6 cells/flask, in a T175 flask in minimal essential medium (α – MEM; Sigma – Aldrich, UK) supplemented with 10% (50mL) foetal bovine serum (FBS; Sigma – Aldrich, UK), 2.4% (12mL) L – glutamine (Sigma – Aldrich, UK) and 1% (5mL) penicillin (Sigma – Aldrich, UK) for three days to reach 80% confluence. The conditioned medium was removed from the flask and 4mL of PBS was added to remove CCM residues. Next, the PBS was removed from the flask and 4mL of Trypsin (Sigma – Aldrich, UK) was added. The flask was placed in the incubator for 10 minutes at 37°C in 5% CO_2 to allow cell detachment. Afterwards, 4mL of fresh growth medium was added to the cell-PBS suspension and collected to a 50 mL tube which was centrifuged for 3 minutes at 1000 rpm in a Mistral 2000 (MSE) centrifuge. The supernatant was removed and the pellet of the cells was suspended in 1 mL of fresh growth medium. Afterwards, the cells were counted with a Neubeuer hemacytometer (Marienfeld) and brought to a concentration of 1 × 10^6 cells/mL. MC3T3s were seeded into a 96 well culture plate (200 µl $well^{-1}$, Nunc, UK) at concentrations of 5,000 cells / well and incubated at 37°C for two hours to allow cell attachment. After that, EVs which were isolated by the fourth and fifth speed at 75,000 x g and 120,000 x g, were added to MC3T3s at four different concentrations (0.5 µg/mL, 1 µg/mL, 5 µg/mL and 10 µg/mL). As a positive control, MC3T3s were cultured in growth medium in the

absence of EVs. This particular experiment has been conducted within a period of three days. After 24 hours (Day 1) Alamar Blue solution was directly added into the culture media at a concentration of 10%. Similarly, after 48 hours (Day 2), Alamar Blue solution was directly added into the culture media at a concentration of 10%. In final day (Day 3) after 72 hours Alamar Blue solution was directly added into the culture media at a concentration of 10%. All absorbances were measured using the microplate spectrophotometer system (Spectra Max-L-Lumi microplate reader) at 525 nm. The results were analysed by the Soft max pro software.

2.4 Gellan Gum (GG) hydrogel

2.4.1 Preparation of Gellan Gum Fluid Gels

In this study eight natural Gellan Gum (GG) hydrogels were prepared (Table 3) with varied polymer and cross-linker concentrations as well as polymer to cross - linker ratio and evaluated as a potential injectable system that may be used to controllably deliver therapeutic doses of isolated EVs. The main idea was to produce a gellan gum fluid gel, which can mimic the rheological behavior of a toothpaste to enable easy injection and maintain the structure locally to facilitate release of incorporated EVs.

Sample Code	GG Concentration	$CaCl_2$ Concentration	Agitator Speed
1	2% w/v	200μL of 50mM	1150 rpm
2	2% w/v	200μL of 100mM	1150 rpm
3	2% w/v	150μL of 50mM	1150 rpm
4	2% w/v	150μL of 100mM	1150 rpm
5	1.5% w/v	200μL of 50mM	1150 rpm
6	1.5% w/v	200μL of 100mM	1150 rpm
7	1.5% w/v	150μL of 50mM	1150 rpm
8	1.5% w/v	150μL of 100mM	1150 rpm

Table 3. Table presenting the design of experiments which were conducted in order to evaluate the effect of gellan gum and cross-linker concentration. The agitator speed was fixed at 1150 rpm for all the gel suspensions.

For each sample, Gellan Gum powder (Sigma – Aldrich) was thoroughly mixed with sterile water under constant stirring and heated progressively to 90°C until full dissolution was achieved. After that, GG gel was stored for 30 minutes at 25°C to cool down. The gel was then sheared for 5 minutes at 1150 rpm using an overhead impeller and calcium chloride (Sigma – Aldrich) was added drop wise. The rheological behavior of the resultant fluid gel was then analysed and compared with a Colgate toothpaste bought from a local pharmacy.

2.4.2 Rheological measurements

All rheological measurements were performed using an AR-1000 rheometer fixed with a stainless-steel cone (angle 2°, diameter of 40 mm) and plate geometry. Dynamic viscosity measurements for all the samples were taken at 37°C using a 5-minute shear continuous ramp from 1 s^{-1} to 1000 s^{-1}. Oscillation frequency sweep measurements were used to determine the rheological behavior of the samples in terms of the elastic modulus (G') and viscous modulus (G") as a function of frequency from 0.01 to 10 Hz. Measurements were taken at 37°C and performed at 1 min equilibrium time and 0.5% strain (linear mode). A sample of toothpaste has been used as positive control due to the product's controllable flow behavior and its recovery characteristics.

2.5 Statistical analysis

The statistical analysis was performed using SPSS 15.0 software (SPSS, Inc., Chicago, IL, USA). The results are expressed as ± standard deviation (SD). A paired t-test was used to identify any significant statistical difference among the means of independent groups. A p-value < 0.05 was considered as statistically significant.

CHAPTER 3 – RESULTS AND DISCUSSION

EVs have attracted considerable interest in the field of tissue engineering due to their capability to mediate cell to cell communication and enable the transfer of genetic information in important biological processes such as angiogenesis, immunomodulation, extracellular matrix interaction and tissue regeneration (Lee *et al*., 2012; De Jong *et al*., 2014; Qin *et al*., 2016; Davies *et al.*, 2017). More specifically, several studies have reported that EVs derived from mesenchymal stem cells (MSC) were able to improve recovery in animal models of experimentally, induced acute renal injury and also promote bone regeneration (Osugi *et al*., 2012; Vicencio *et al*., 2015).

However, the identification of these population is problematic due to the variety of isolation and characterisation protocols and also the continuing development of EVs biogenesis. More and more studies have been conducted to purify EVs and several methods have been applied, including ultracentrifugation, ultrafiltration, size exclusion chromatography, polymer - based precipitation and immunoaffinity separation (Lai *et al*., 2011; Momen-Heravi *et al.,* 2013; Witwer *et al*., 2013; Zaborowski *et al*., 2015; Yakimchuk, 2015; Szatanek *et al*., 2015; Zhou *et al*., 2016). So far, differential centrifugation coupled to ultracentrifugation is the most widely used method for EVs isolation from cell conditioned media (CCM) and various biological fluids. Notably, the effects of repeating ultracentrifugation steps on the recovery of EV yields have not been evaluated comprehensively. There are many isolation protocols that differentiate in the number of steps and the conditions of centrifugation such as rotor types. Thus, the results obtained using dissimilar protocols make the comparison difficult (Konoshenko *et al*., 2018). It appears that a unified protocol which will enable an efficient isolation and characterisation of EVs is needed.

The aim of this study was to assess and compare the various osteoblastic EVs factions that were isolated from conditioned culture media (CCM) using two different isolation protocols and applying five different centrifugation forces with the view of selecting a protocol tailored to a specific population and consequently contribute to the optimisation of ultracentrifugation method.

These two protocols, namely sequential and differential, have been compared based on the size, concentration and protein content of isolated EVs in order to identify similarities and differences which might lead to the most efficient one.

Both isolation protocols (sequential and differential) consist of five equal speeds starting from 10,000 x g and then accelerating gradually to 20,000 x g, 50,000 x g, 75,000 x g and finally to 120,000 x g. The difference between these two protocols lies on the centrifugation of the supernatant. During the sequential protocol the initial supernatant was centrifuged consecutively at all spins whereas at the differential protocol, five tubes of supernatants were centrifuged individually at all five spins. The biophysical properties of isolated EVs, such as sizes, concentrations and morphologies, were obtained by using dynamic light scattering (DLS) analysis, nanoparticle tracking analysis (NTA) and transmission electron microscopy (TEM). A BCA protein assay was also conducted to assess the protein content of isolated EVs for each spin separately. In addition, the influence of osteogenic EVs on MC3T3 cells metabolic activity was examined for a period of three days in both protocols, after culturing cells with four different doses of EVs isolated by the last two spins.

3.1 Dynamic light scattering analysis (DLS)

DLS was used to evaluate the size distribution of osteoblastic EVs isolated by sequential and differential ultracentrifugation at five different centrifugation forces. The analysis of DLS findings of the sequential protocol showed that the majority of EVs sizes range from 50 to 260 nm (Figure 20b) whereas the analysis of DLS findings of the differential protocol, showed that the majority of EVs sizes range from 50 to 794 nm (Figure 21b). More specifically, at the first spin of sequential protocol, at 10,000 x g, the average size and scattering intensity of EVs was reported to be of 260 ± 16.1nm, 17% while at the same spin in differential protocol the average size of EVs was reported to be higher, 449 ± 14 nm having a slightly lower scattering intensity of 15%. At the next two sequential spins the average size and scattering intensity of EVs decreased cumulatively to 247.5 ± 17.7 nm, 14.4% and 198.4 ± 15 nm, 13% respectively.

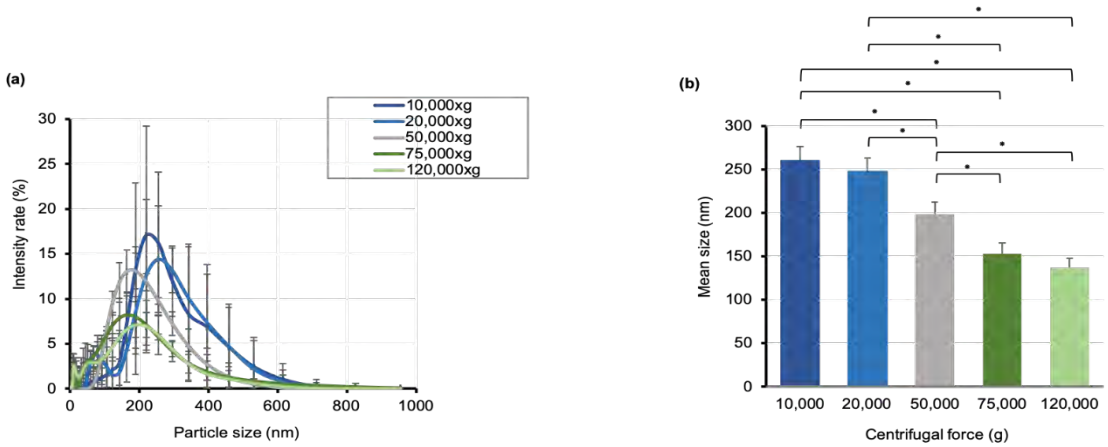

Figure 20. Dynamic light scattering analysis of isolated EVs by the sequential method. (a) Size distribution curve including standard deviation calculated from n=5. (b) Statistical analysis among the average sizes (nm) of isolated EVs including standard deviation calculated from n=5.

On the other hand, in the corresponding differential spins it was observed that the average size and scattering intensity of EVs increased unexpectedly to 513 ± 13 nm, 19% and 794 ± 15 nm, 21%. At the last two sequential spins the average size and scattering intensity of EVs further decreased to 152.9 ± 14.6 nm, 8.8% and 147.4 ± 13.6 nm, 7%. Similarly, at the last two differential spins the average size and scattering intensity of EVs decreased to 249 ± 11.5 nm, 10% and 129 ± 11 nm, 2.4%. It is interesting that in the case of sequential protocol between the last two centrifugal forces there was no significant change in size and intensity profile while the opposite happened in differential protocol. It is important to recognise that the scattering intensity of EVs isolated by the last differential spin was significantly lower than all other samples in both protocols. Despite the size variation that exists in the sample, no statistical differences ($p > 0.05$) between the average size of isolated EVs by the first two sequential spins; 10,000 x g and 20,000 x g, was detected (Figure 20b). However, further increase in the centrifugal force significantly ($p < 0.05$) decreased the EVs mean size (Figure 20b). Similarly, in the case of differential protocol no statistical differences ($p > 0.05$) were observed between the average sizes of the first two differential spins (Figure 21b), however further increase in the centrifugal force significantly ($p < 0.05$) decreased the EVs mean size (Figure 21b).

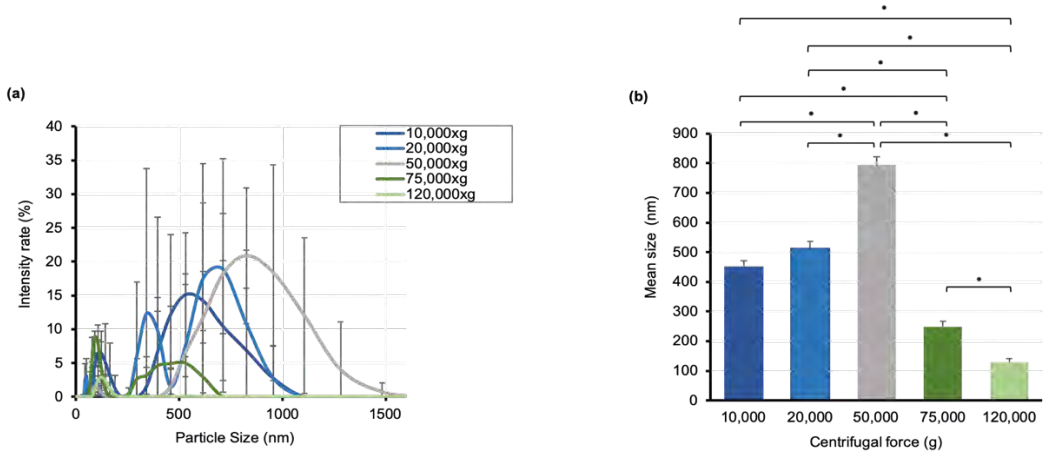

Figure 21. Dynamic light scattering analysis of isolated EVs by the differential method. (a) Size distribution curve including standard deviation calculated from n=5. (b) Statistical analysis among the average sizes (nm) of isolated EVs including standard deviation calculated from n=5.

Overall, it was observed that in the case of sequential protocol, the size and the scattering intensity of the EVs decreased when the speed of isolation gradually increased. Two subpopulations exist in all the centrifugal forces and this can be attributed to the nature of the differential protocol. In the case of differential protocol, the size and the scattering intensity of the EVs increased during the first three spins while the opposite happened in the last two spins, meaning that EVs' size and finally scattering intensity decreased, potentially due to errors introduced by the DLS or breakage of larger EVs at the last two high centrifugal forces. It was also observed that the sizes and scattering intensity of EVs were greater in the differential protocol compared to the sequential; this applies for the first four spins while on the fifth spin the two protocols have similar average sizes (147.4 ± 13.6 nm, 129 ± 11 nm). Previous studies have been shown that EVs isolated from CCM by differential ultracentrifugation consisted from three main sequential spins (last speed at 100,000 x g and 120,000 x g) had an average size of EVs < 200 nm (Palmieri *et al*., 2014; Martins *et al*., 2016; Davies *et al*., 2017). The aforementioned findings appear to be similar with the findings observed in the last two spins of both protocols, sequential and differential conducted in this study. It must also be recognized that high standard deviations were associated with all the DLS measurements. This fact indicates that at all spins in both protocols the EV suspensions had a wide range of sizes. This fact confirms the heterogenous population that exists in EV suspensions as previously

reported in the literature (Momen-Heravi *et al.,* 2013; Yuana *et al*., 2013; Lamichhane *et al.*, 2014; Zaborowski *et al*., 2015; Mendes *et al.,*2016; Willms *et al*., 2018; Azoidis *et al*., 2018).

3.2 Nanoparticle tracking analysis (NTA)

A Nanosight LM10 instrument was also used to analyse further the size distribution and evaluate the concentration of EVs for both protocols at each spin. The analysis of NTA findings revealed that the majority of EV sizes at all spins in both protocols range from 50 to 200 nm (Figure 22a and Figure 23a). During the first spin in both protocols, the isolated EVs reported to have similar average sizes but slightly different concentrations (Figure 22b and Figure 23b).

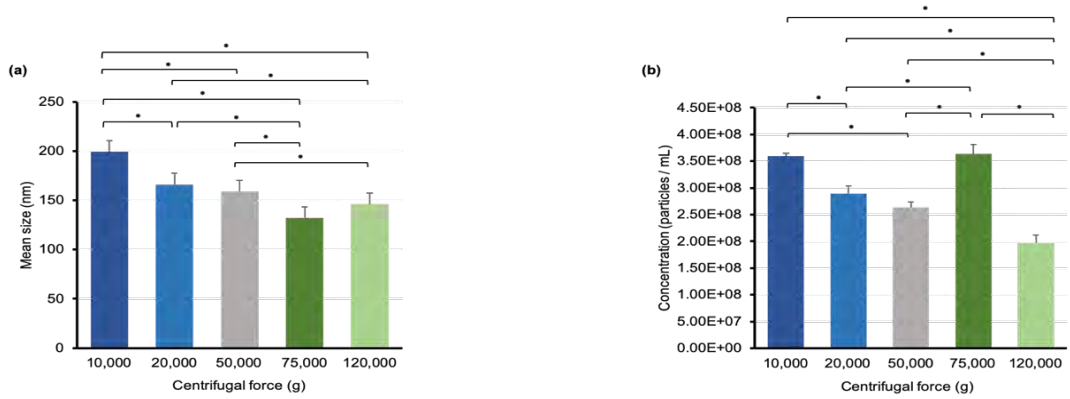

Figure 22. Nanoparticle tracking analysis of isolated EVs by the sequential method. (a) Statistical analysis among the average sizes (nm) of isolated EVs including standard deviation calculated from n=5. (b) Statistical analysis in average concentrations (particles/mL) of isolated EVs.

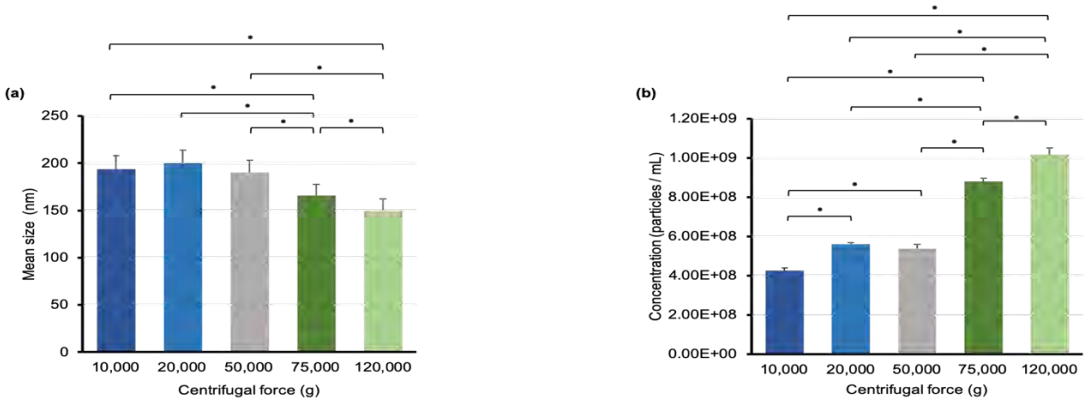

Figure 23. Nanoparticle tracking analysis of isolated EVs by the differential method. (a) Statistical analysis among the average sizes (nm) of isolated EVs including standard deviation calculated from n=5. (b) Statistical analysis in average concentrations (particles/mL) of isolated EVs.

In sequential protocol, the average size and concentration of EVs stated to be 199.6 ± 16 nm, 3.60 x 10^8 particles/mL whereas at the same spin in differential protocol, the average size and concentration of EVs stated to be 194 ± 17.5 nm, 4.25 x 10^8 particles/mL. Passing through the second spin at 20,000 x g, the average size and concentration of EVs in sequential protocol decreased significantly to 166 ± 15.5 nm, 2.89 x 10^8 particles/mL in contrast to the differential protocol where the size and concentration of EVs slightly increased to 200 ± 17 nm, 5.6 x 10^8 particles/mL. During the third speed at 50,000 x g, in both protocols, the average size and concentration of EVs were slightly decreased to 159 ± 15.6 nm, 2.74 x 10^8 particles/mL and 190 ± 16 nm, 5.38 x 10^8 particles/mL. A significant increase ($p < 0.05$) in concentration of EVs was observed for both protocols at the fourth spin of 3.64 x 10^8 particles/mL and 8.81 x 10^8 particles/mL respectively. Despite the fact that the concentration of EVs was increased, the size of EVs was decreased to 132 ± 15.3 nm and 165.7 ± 17.3 nm respectively. At the last spin the average size of EVs are not significantly different between the two protocols (Table 4 and Figures 22a and 23a). More specifically, EVs isolated after the sequential protocol, were found to have an average size of 148 ± 15 nm. Similarly, EVs isolated after the differential protocol were reported to have an average size of 150 ± 14.6 nm. However, at this particular spin, the EV concentrations were significantly different between the two protocols. Interestingly, in the case of sequential protocol, the EVs concentration derived at last spin (120,000 x g) was significantly lower than other fractions even 75,000 x g that resulted in a similarly sized population. On the other hand, in the case of differential protocol, the concentration derived at the 120,000 x g was significantly higher than other fractions. It is also notable that at the last spin EV concentrations in differential protocol was significantly higher than the sequential, 10.18 x 10^8 particles/mL and 1.97 x 10^8 particles/mL, respectively.

Significant statistical differences ($p > 0.05$) in the average size and concentration of EVs were observed among the five sequential spins (Figures 22a and 22b). Similar to sequential protocol, significant statistical differences ($p > 0.05$) in the average size and concentration of EVs were observed among the five differential spins (Figures 23a and 23b).

The significant statistical differences which observed among the measurements of average sizes of isolated EVs and also the high standard deviation associated with these measurements reveals the heterogeneity of EVs population (Momen-Heravi *et al.,* 2013; Yuana *et al*., 2013; Lamichhane *et al.*, 2014; Zaborowski *et al*., 2015; Mendes *et al.,*2016; Willms *et al*., 2018; Azoidis *et al*., 2018).

Overall, EVs characterisation using the NTA instrument revealed that in the case of sequential protocol, the sizes and concentrations of EVs decreased when the speed of isolation gradually increased, except the fourth spin during which the concentration of EVs unexpectedly increased (Figure 22). Similarly, in the case of differential protocol, the sizes of EVs decreased when the speed of isolation gradually increased, however, the concentrations gradually increased (Figure 23). The fact that no statistical difference was observed in the mean size with the increase in spin between 20,000 x g and 50,000 x g for both the sequential and differential protocols could be attributed to the higher concentration of EVs with even smaller sizes that were pelleted at even higher spins; 75,000 x g, and due to differences in the EVs density. In previous studies, osteoblast-derived EVs isolated from CCM by differential ultracentrifugation and characterised by NTA instrument have been concluded with an average diameter below 160 nm (Morhayim *et al*., 2016; Davies *et al*., 2017). The aforementioned findings appear to be similar with the findings observed in the last two spins of both protocols, sequential and differential conducted in this study.

The comparison of DLS and NTA measurements reveals that the EVs measured by DLS instrument appeared to have greater average sizes than the EVs measured by the NTA instrument. This was observed especially during the implementation of differential protocol. Interestingly, at the first speed at 10,000 x g a significant difference in size was observed. This unexpected finding might have happened due to DLS inability to resolve accurately samples with heterogeneous population and its tendency to miscalculate the contribution of the larger particle at the intensity of the scattered light which is used for correlation with the particle diameter (Serrano-Pertierra *et al*., 2019).

In that respect, NTA appears to be more effective since, according to the findings, the average sizes emerged from sequential protocol did not have major differences from the respective sizes which emerged from differential protocol. NTA has another advantage, that is, its detection limits are lower and close to the EVs sizes; therefore the measurements are more accurate and the results are in better agreement with the TEM ones (Figure 24) (Malvern Panalytical, 2019). It is interesting that both instruments, DLS and NTA, revealed that at the last two spins in both protocols, EVs with similar average sizes appeared. These have a mean diameter below 300 nm correlating with diameters previous documented for small EVs and exosomes (Xiao *et al*., 2007; De Jong *et al*., 2014; Yáñez-Mó *et al*., 2015; Zaborowski *et al*., 2015; Bruno *et al.*, 2016; Ha *et al*., 2016; Szatanek *et al*, 2017; Konoshenko *et al*., 2018; Harjes *et al*., 2019). However, it is notable that in differential protocol significantly higher EV concentrations were detected at all spins compared to sequential, especially at the last two spins. Previous studies mentioned that high - speed spins in EV purification not only increase the purity of target EVs but also decrease their yield and quality since aggregated EVs can be observed in samples obtained by ultracentrifugation (Théry *et al*., 2006; Konoshenko *et al*., 2018). Thus, the high concentration samples that occurred by the differential ultracentrifugation method might be associated with aggregated vesicle population and lipoproteins.

	DLS		NTA	
	Mean size (nm)	**Intensity (%)**	**Mean size (nm)**	**Concentration (x 10^8 particles/mL)**
SEQUENTIAL PROTOCOL				
10,000 x g	260 ± 16.1	17	199.6 ± 16	3.60
20,000 x g	247.5 ± 17.7	14.4	166 ± 15.5	2.89
50,000 x g	198.4 ± 15	13	159 ± 15.6	2.74
75,000 x g	152.9 ± 14.6	8.8	132 ± 15.3	3.64
120,000 x g	147.4 ± 13.6	7	148 ± 15	1.97
DIFFERENTIAL PROTOCOL				
10,000 x g	449 ± 14	15	194 ± 17.5	4.25
20,000 x g	513 ± 13	19	200 ± 17	5.60
50,000 x g	794 ± 15	21	190 ± 16	5.38
75,000 x g	249 ± 11.5	10	165.7 ± 17.3	8.81
120,000 x g	129 ± 11	2.4	150 ± 14.6	10.18

Table 4. Table presenting an overview of EV sizes, intensity rates and concentrations obtained from DLS and NTA instruments at all spins in both protocols.

3.3 Transmission electron microscopy (TEM)

Electron microscopy (EM) was necessary for this study to further characterise EVs sizes and also to visualise their morphology. Taking into consideration that in the last two spins similar average sizes emerged, TEM was decided to be used in order to capture the EV sizes and morphologies isolated by the sequential and differential protocols at 75,000 x g and 120,000 x g. Figures 24A and 24C demonstrate the presence of EVs with a diameter above and below the average size particles isolated by the last two sequential spins. Similarly, Figures 24B and 24D demonstrate the presence of EVs with a diameter above and below the average size particles isolated by the last two differential spins. In both protocols it was observed a heterogeneous population of EVs with spherical morphologies and electron dense membranes, correlating with morphologies previously documented for small EVs and exosomes (Wu *et al*., 2017; Vestad *et al*., 2017).

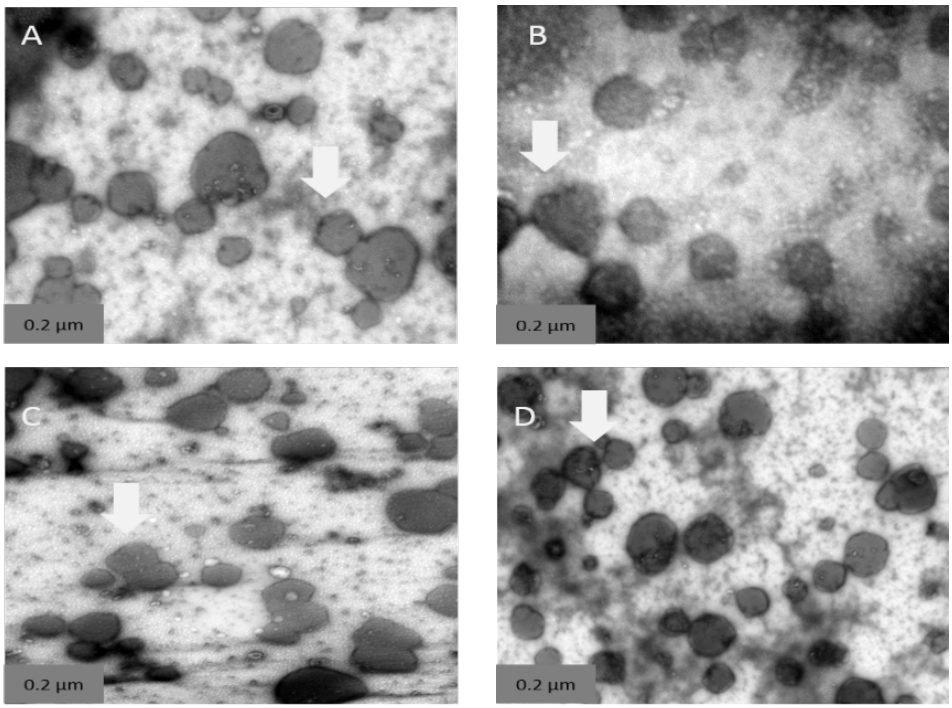

Figure 24. TEM images of negatively stained EVs. The images show (A) MC3T3s derived EVs isolated by the sequential protocol at 75,000 x g, (B) MC3T3s derived EVs isolated by the differential protocol at 75,000 x g, (C) MC3T3s derived EVs isolated by the sequential protocol at 120,000 x g, (D) MC3T3s derived EVs isolated by the differential protocol at 120,000 x g. All images show the presence of EVs in several sizes and also the presence of aggregated EVs (white arrows).

The electron dense membrane of the EVs interacted strongly with electrons in TEM and therefore the purified vesicles look darker (Figure 24A, 24B, 24C and 24D) (Yuana *et al*., 2013; Van der pol *et al*., 2014; Zabeo et *al*., 2017). Interestingly, the EVs aggregations are obvious in all the figures above (white arrows) but more specifically in figure 24D which represents the more concentrated sample according to the NTA findings for the highest spin; 120,000 x g. This was also confirmed by the higher mean EVs size in the case of the sequential protocol at the highest spin in comparison to 75,000 x g. Overall the increase in spin decreases the EVs size. During the sample preparation of this experiment, there is a likelihood of emergence of several inorganic salts which eventually will form aggregates. The inorganic salts may cause reduction and non-uninform adhesion of EVs on the copper grid surface and render the analysis more complicated. The inorganic salts could be eliminated by reducing the amount of PBS in stored pellets of EVs in future protocols.

3.4 Bicinchoninic acid assay (BCA)

The next stage of EVs characterisation concerns the biochemical profile of EVs. Several studies have been conducted to characterise the protein content of isolated EVs. One of the most frequently used method is the Bicinchoninic acid assay (BCA) or Bradford assay. In this study BCA protein assay kit (Thermo scientific, USA) was used in order to obtain an initial view of the protein content of osteoblast-derived EVs. The total protein content of isolated EVs was determined for all spins by a BCA standard protocol. Absorbance units were measured using a micro-plate reader for both methods of isolation. Figure 25 presents the protein concentration of MC3T3 cells cultured in the absence of EVs.

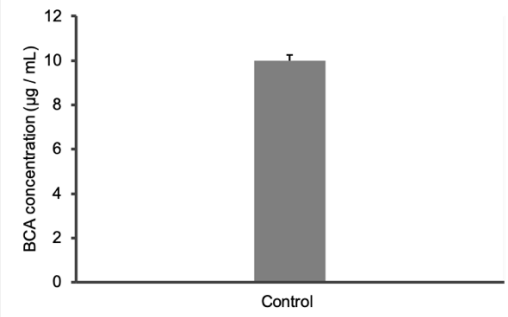

Figure 25. Positive control graph. The evaluation of protein content in MC3T3 cells cultured without the presence of EVs. BCA concentration of MC3T3s reported to be 10.2 ± 5 µg/mL.

Figure 26 presents the protein concentration calculated from the raw absorbance measurements using a calibration curve for the sequential and differential protocol.

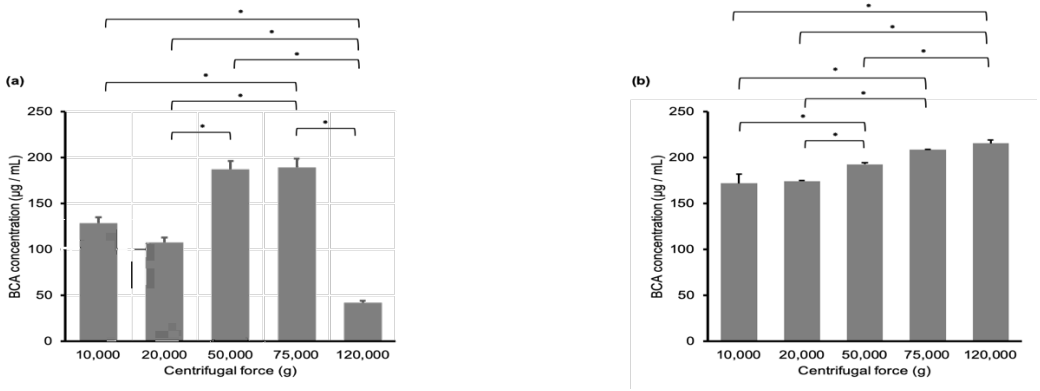

Figure 26. Precipitated extracellular vesicles released from MC3T3 cells were analysed for the content of protein. (a) Statistical analysis in protein content of isolated EVs by the sequential protocol. (b) Statistical analysis in protein content of isolated EVs by the differential protocol.

At the first spin of sequential protocol the BCA concentration of EVs reported to be 128 ± 12 µg/mL while at the same spin in differential protocol reported to be higher reaching 171 ± 18 µg/mL. Following, in the second spin of the sequential protocol, BCA concentration was observed to decrease to 107 ± 10 µg/mL while at the differential protocol the BCA concentration of EVs was slightly increased to 174 ± 3 µg/mL. During the third spin of both protocols the BCA concentrations were observed to increase significantly ($p < 0.05$) to 187 ± 15.5 µg/mL and 192 ± 5 µg/mL respectively. In the next spin of sequential protocol the BCA concentration of EVs increased by 2 units to 189 ± 13.5 µg/mL while in differential protocol increased by 16 units to 208 ± 3 µg/mL. Concluding, at the final spin of sequential protocol, the BCA concentration significantly decreased ($p < 0.05$) to 38.4 ± 9.5 µg/mL compared to differential where the BCA concentration of EVs increased further to 215 ± 5 µg/mL. Notably, no significant difference between the first two sequential spins at 10,000 x g and 20,000 x g was detected. Statistical differences were observed among the first two spins, the third and fourth. Notably, significant statistical differences were observed among the last spin at 120,000 x g and the first four.

Similarly, no significant difference between the first two differential spins at 10,000 x g and 20,000 x g was detected. Significant statistical differences were observed among the last spins, 75,000 x g and 120,000 x g, and the first three.

Overall, it was observed that in both protocols the BCA concentrations were significantly higher than the control (Figure 25 and Figure 26). This is an indication that EVs are rich in proteins which previously has been documented in several studies (Raposo and Stoorvogel, 2013; Yanez-Mo *et al*., 2015). In the case of differential protocol the BCA concentration of EVs increased when the speed of isolation gradually increased, following a similar pattern as the EVs concentration (Figure 23), and concluded to a BCA concentration of 215 ± 5 μg/mL. On the other hand, in the case of sequential protocol, the BCA concentration of EVs cumulatively increased by the fourth spin, following a similar pattern as the EVs concentration (Figure 22), and decreased at the last resulting to a significantly lower BCA concentration than the differential protocol. Notably, at the fourth spin of both protocols, the BCA concentrations of EVs are close. However, at the last spin the BCA concentrations of EVs appeared to have a significant difference; the protein content in sequential protocol is much lower than the differential, as most EVs were most possibly collected at the lower centrifugal forces. The results show that the BCA concentration is a good indication of the EVs isolated concentration. Concluding, the protein concentrations observed in both protocols - especially in differential protocol - were greater than the protein concentration findings reported in relevant studies (Martins *et al*., 2016; Borosch *et al*., 2017). This fact might be associated with the high concentrated samples that were obtained by NTA measurements.

3.5 Alamar Blue Assay (AB)

Recent studies have reported that EVs are involved in the differentiation and proliferation process of cells. According to Morhayim *et al*. (2016), EVs isolated from pre-osteoblasts were able to deliver genetic cargo such as miRNAs that was able to increase the differentiation of embryonic stem cells (ESCs). Similarly, Qin *et al*. (2016), showed that bone marrow stromal/stem cell (BMSC) derived EVs stimulated osteogenic gene expression and osteoblast differentiation in vitro experiments.

Taking into consideration the findings of these studies, the influence of osteoblast-derived EVs was examined for a period of three days, after culturing MC3T3 cells with four different doses of EVs (0.5μg, 1μg, 5μg, 10μg), isolated by both protocols at the last to spins (75,000 x g and 120,000 x g). As a positive control, MC3T3s were cultured in growth medium in the absence of EVs. The effect of EVs dosing on cells' metabolic activity have been evaluated using an Alamar Blue assay (AB) according to the standard protocol as described in Chapter 2. AB assay is used to measure quantitatively the proliferation of various human and animal cell lines, bacteria and fungi (Bora *et al*., 2009; Rampersad, 2012). Analysing the findings of the sequential protocol revealed that the addition of EVs isolated at 75,000 x g and 120,000 x g, increased the cells' proliferation. In day 1 MC3T3s appeared to proliferate gradually in the presence of EVs isolated using both spins. Significant statistical differences were observed among the control cells and the cells with EVs isolated using the two sequential and differential spins (Figures 27a and 27d).

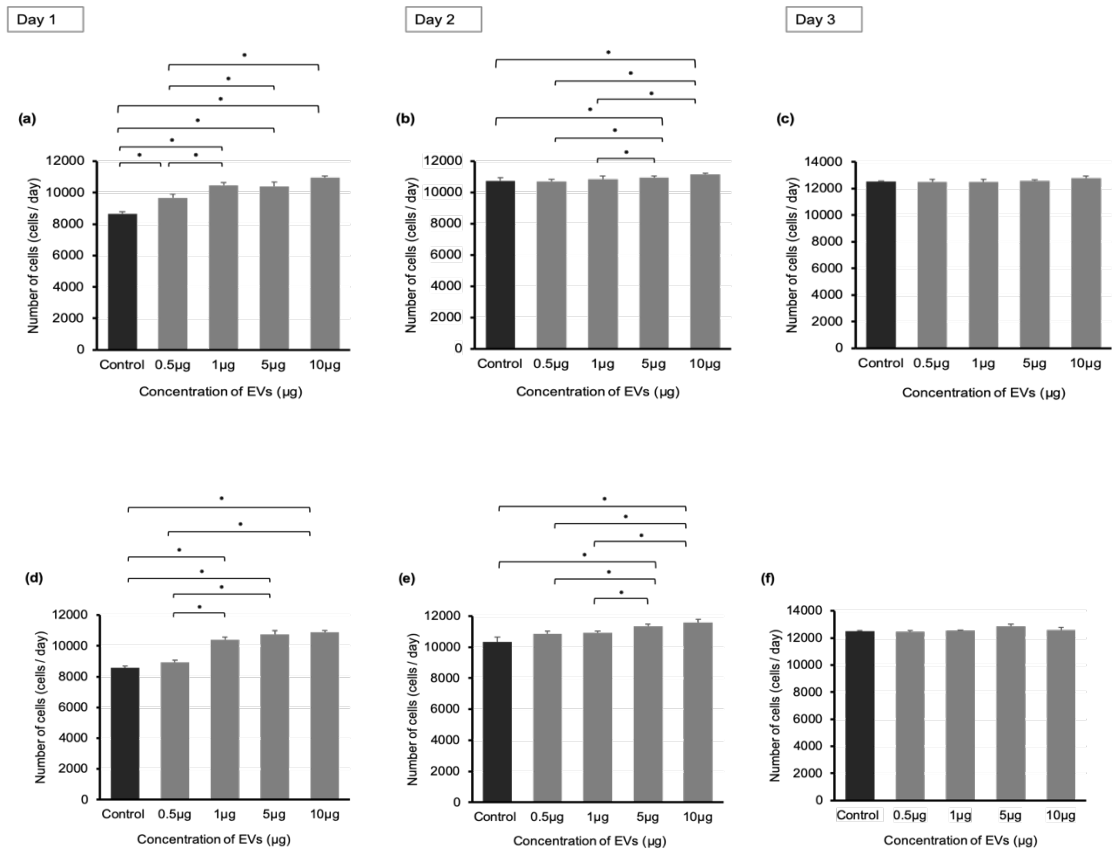

Figure 27. MC3T3s proliferation was examined for 3 days after culturing cells with four different concentrations (0.5μg, 1μg, 5μg, 10μg) of isolated EVs by the sequential protocol at 75,000 x g (a, b, c) and 120,000 x g (d, e, f).

More specifically, significant statistical differences were observed among the dose of 0.5μg and the other doses of EVs. It is clear that the doses of 1μg, 5μg and 10μg significantly increased the MC3T3s proliferation in both sequential spins in day 1. Following, in day 2 MC3T3s appeared to proliferate gradually in both spins having equivalent proliferation rates (Figure 27b, and 27e). Significant statistical differences were observed among the last two doses of EVs (5μg and 10μg) and the control. The doses of 5 μg and 10 μg significantly increased the cell proliferation in both sequential spins in days 1 and 2. It is notable that, in day 3, the cells had apparently reached the highest values of proliferation therefore there are no significant statistical differences between the control and the cultures with the presence of EVs ($p > 0.05$). This fact indicates that the addition of EVs in cell cultures did not significantly enhanced the cells' proliferation beyond day 1 and 2.

As expected, the analysis of findings in the case of differential protocol revealed that the addition of EVs in cultures isolated at 75,000 x g and 120,000 x g increased significantly the cells' proliferation (this applies for all three days) in all doses especially in the case of 5μg and 10μg. Interestingly, in day 1 all the doses of EVs significantly increased cells' proliferation in both protocols. More specifically, EVs in dose of 10μg appeared to be more efficient for cells since increased significantly the cells proliferation compared with the other doses in both spins as shown in Figure 28a and 28d. In day 2 and 3 MC3T3s appeared to have significantly high values of proliferation in both spins ($p < 0.05$). More specifically, EVs in dose of 5μg and 10μg appeared to be more efficient compared with the other doses for both spins.

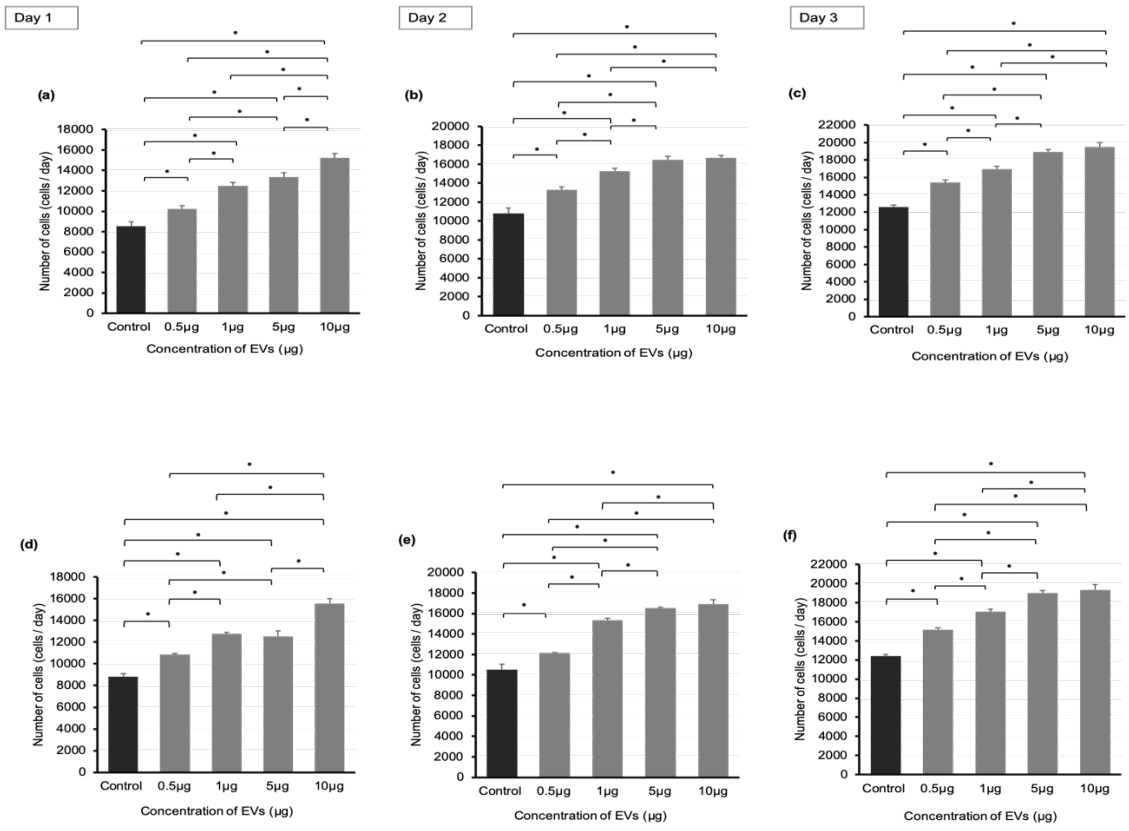

Figure 28. MC3T3s proliferation was examined for 3 days after culturing cells with four different concentrations (0.5μg, 1μg, 5μg, 10μg) of isolated EVs by the differential protocol at 75,000 x g (a, b, c) and 120,000 x g (d, e, f).

According to the findings, the addition of EVs isolated by the differential protocol in cells' cultures enhanced the cells' proliferation more than in the case of the EVs isolated using the sequential method. The EVs' doses of 5μg and 10μg seem to be more efficient since those significantly enhanced the cells' proliferation. The comparison between the sequential and differential at both spins reveals that the EVs isolated by the differential protocol had a positive effect in cellular activity since it seems that 10 μg enhance cells proliferation to a greater extend in comparison that the ones isolated from the sequential protocol ($p < 0.05$) (Figures 27 and 28). An explanation as to why the increase EVs concentration isolated using the sequential method did not enhance cell proliferation could be that those EVs went through a number of centrifugation cycles and therefore their quality at high spin was reduced in comparison to the ones isolated using the differential method.

A comparison of all processes which were performed on culture media – derived EVs revealed that differential ultracentrifugation generated the highest EVs yield. In this case, high in concentration and protein content samples have been isolated. Interestingly, at the last two spins (75,000 x g and 120,000 x g) in both protocols, EVs with similar average sizes appeared. This is an indication that the fifth spin at 120,000 x g could be replaced by the fourth spin at 75,000 x g in future protocols and thus reduce the number of damaged vesicles which are associated with the high - speed spins and increase their quality. Overall, the differential protocol seems to be more effective for EVs isolation, however the purified EVs presence in both protocols need to be confirm in an exhaustive manner in further studies. Also, regarding the EVs characterisation, the NTA instrument seems to be more effective than DLS since measure each vesicle separately while DLS tend to miscalculate the contribution of the large vesicles. Also, NTA detection limits are lower than DLS and close to the EVs sizes; therefore there is a low possibility to measure large in size particles and eventually the averaged data in a sample cannot be affected.

3.6 Gellan Gum (GG) characterisation and therapeutic potential of encapsulated EVs

EVs have the potential to be used as therapeutic delivery carriers and could be uniquely employed in regenerative medicine. They have important advantages on therapeutic application regarding the regulatory and safety concerns (Lamichhane *et al.*, 2014; De Jong *et al.*, 2014). However, there is one major obstacle in the therapeutic application of isolated EVs that is to target EVs to a particular therapeutic location and maintain an effective dose at that location hence that localised pathologies to be treated (Nikravesh *et al.*, 2019). In that respect a range of natural hydrogels such as Alginate and Chitosan, have been used as a delivery vehicle capable to locally release therapeutic molecules. Of these hydrogels, Gellan Gum gels have received a great attention due to their physical gelation properties (Kretlow *et al.*, 2007; Lanza *et al.*, 2014; Radhakrishnan *et al.*, 2016; Kowalczewski and Saul, 2018).

In this study, eight natural Gellan Gum (GG) hydrogels (Table 3) were prepared with varied polymer and cross-linker concentrations and evaluated as a potential injectable system that may be used to controllably deliver therapeutic doses of isolated EVs. In order to guide what rheological behavior would be desirable for an injectable agent, toothpaste was considered as a baseline material (positive control) to compare material behaviors. This is because toothpaste exhibits shear thinning behavior that enables easy injection. Figure 29 shows the viscosity measurements obtained for all the samples in comparison to the control.

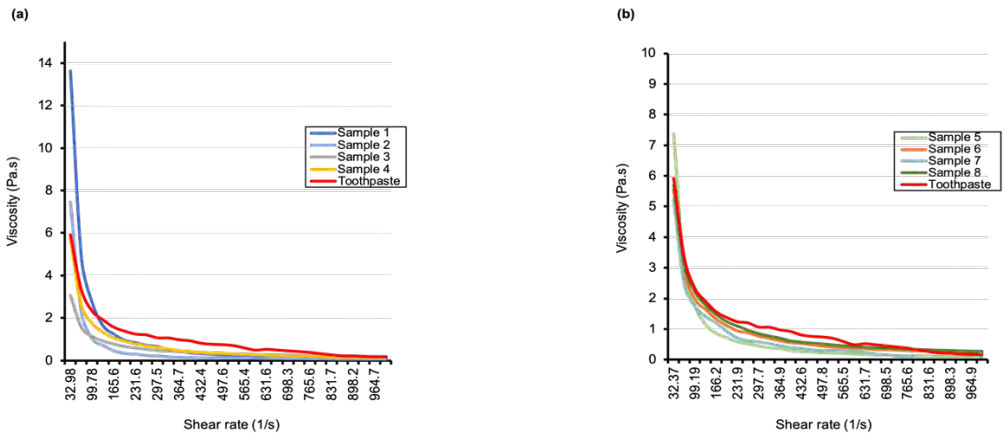

Figure 29. Rheological characterisation of gellan gum (GG) gel suspensions at 37℃. (a) Viscosity measurements for the 2%w/v GG gel suspensions. (b) Viscosity measurements for the 1.5%w/v GG gel suspensions.

All the manufactures samples were found to exhibit shear thinning behavior. The sample 4, made of 2% w/v GG 150µL $CaCl_2$ (100mM), and sample 8, made of 1.5%w/v GG 150µL $CaCl_2$ (100mM) have been found to give viscosity data closer to the positive control. This behavior is appropriate within injectable systems since lower force is required enabling easy injection. Following these initial findings, the viscoelasticity of these samples was assessed. Figure 30 shows the mechanical data obtained for frequency as function of storage modulus (G') and loss modulus (G"), for both samples in comparison to the control. Storage modulus (G') is a measure of elastic response (stored energy) of a gel while the loss modulus (G") is a measure of viscous response (energy lost as heat) of a gel (Khedmat *et al.*, 2013). Sample 8 (1.5%w/v GG 150µL $CaCl_2$ (100mM)) exhibited lower G' and G" values, more similar to the control. It is clear that the G' and G" values of sample 8 is higher than the toothpaste. This is directly related to the extent of cross-linking. The higher the degree of cross-linking the greater the storage modulus presented in suspension. Thus, GG gels with lower degree of cross-linking need to be manufactured and investigated further for the encapsulation and the delivery of osteoblastic EVs.

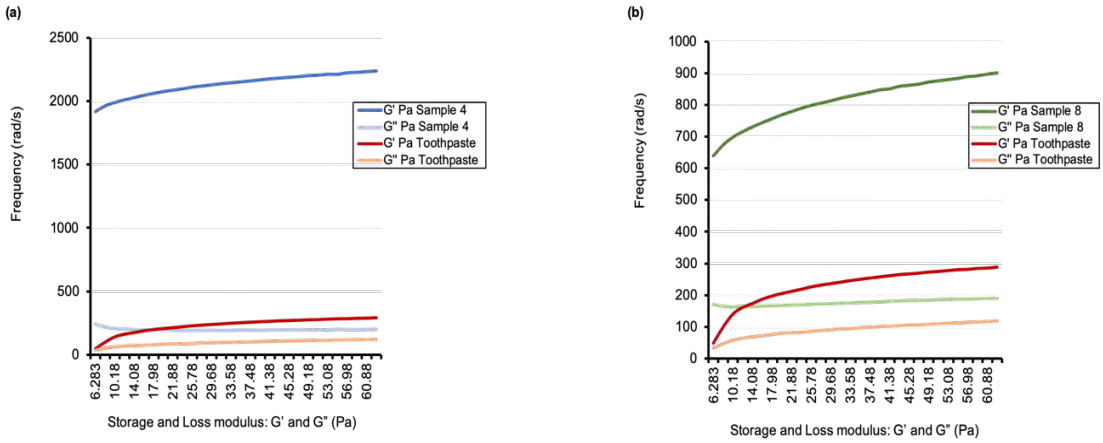

Figure 30. Rheological characterisation of gellan gum (GG) gel suspensions at 37℃. (a) Frequency sweep measurement for sample 4 (2%w/v GG 150µL $CaCl_2$ 100mM). (b) Frequency sweep measurement for sample 8 (1.5%w/v GG 150µL $CaCl_2$ 100mM).

CONCLUDING REMARKS

The natural capability of EVs both microvesicles and exosomes to deliver biological cargo has attracted attention since they could be used as a delivery vehicle for osteoinductive proteins and nucleic acids that are highly effective in bone regeneration technologies. However, the identification of these population is a difficult task for the researchers due to the variability that exists in EVs sizes, way of formation, source and also the variety of isolation and characterisation protocols.

This study aimed to contribute to the optimisation of ultracentrifugation method towards the isolation of EVs. In that respect, two ultra - centrifugation protocols (sequential and differential) consisting of five centrifugal forces were investigated in order to assess the osteoblastic EVs population that emerge from each spin; with emphasis on sizes, concentrations and morphologies using DLS, NTA and TEM instruments. EVs characterisation using DLS instrument revealed that in the case of sequential protocol, the size of EVs decreased when the speed of isolation gradually increased. In the case of differential protocol, the size of EVs increased during the first three spins while the opposite happened in the last two. Similarly, EVs characterisation using NTA instrument revealed that in the case of sequential protocol, the size and concentrations of EVs decreased when the speed of isolation gradually increased, except the fourth spin that EVs concentration increased. In the case of differential protocol, the sizes of EVs decreased but the concentrations increased when the speed of isolation gradually increased. In general, EVs measured by DLS instrument appeared to have greater average sizes than the EVs measured by NTA instrument. This was observed especially during the implementation of differential protocol. Interestingly, at the first speed at 10,000 x g a significant difference in size was observed. This unexpected finding might have happened due to DLS inability to resolve accurately samples with heterogeneous population and its tendency to miscalculate the contribution of the larger particle at the intensity of the scattered light which is used for correlation with the particle diameter. In that respect, NTA appears to be more effective since, with lower detection limits that are close to the EVs sizes, making NTA a more accurate method for EVs size measurements, that provides results similar to that obtained by the TEM.

Overall, it was shown that high concentration EV suspensions with high protein content were isolated after the implementation of differential protocol. It was observed that, at the last two centrifugal forces (75,000 x g and 120,000 x g) in both protocols, EVs with similar average sizes appeared, providing an indication that the last speed at 120,000 x g could be replaced by the 75,000 x g speed in future protocols. This may help to maintain EV integrity, which may be important in using these nanoparticles for regenerative therapies. Observation of similar sizes EVs obtained at different centrifugal forces could be attributed to EVs having varying densities.

The influence of EVs on cellular metabolic activity was assessed for a period of three days. The findings showed that the addition of EVs isolated by the differential protocol had a positive effect in cellular activity since it seems to enhance cells proliferation. Overall, the differential protocol seems to be more effective for EVs isolation. However, the purified EVs presence in both protocols need to be confirm in an exhaustive manner in further studies. In conclusion, gellan gum (GG) fluid gels were prepared and evaluated as a potential injectable system that may be used to deliver therapeutic doses of EVs. It was reported that gellan gum gels made of 2% w/v GG 150µL $CaCl_2$ (100mM) and 1.5% w/v GG 150µL $CaCl_2$ (100mM) found to give mechanical data closest to the positive control. These two samples need to be investigated further for the production of a localised vehicle for EVs release.

EVs have important effects in biology and may be useful as delivery vehicles of therapeutic agents. Despite the effort to characterise comprehensively the EVs in this study, many challenges remain before engineered EVs for delivery applications. This includes further work to test the efficacy of vesicles released from the gellan gum formulations optimised in this thesis. Further, to enable these acellular vesicle products to become therapies the large-scale production of EV will be required. The resolution of the above considerations alongside the continuous evolvement of EVs as therapeutic delivery vehicles might lead to new therapeutic prospects which will involve EVs in regenerative and bio-engineering therapies in future.

LIST OF REFERENCES

1. Ahmed, E. (2015). Hydrogel: Preparation, characterization, and applications: A review. *Journal of Advanced Research*, 6(2), pp.105-121.
2. Anderson, H.C. (1967). Electron microscopic studies of induced cartilage development and calcification. *The Journal of cell biology*, 35(1), pp.81-101.
3. Apolinário, A., Magoń, M., Pessoa Jr, A. and Rangel-Yagui, C. (2018). Challenges for the Self-Assembly of Poly (Ethylene Glycol)–Poly (Lactic Acid) (PEG-PLA) into Polymersomes: Beyond the Theoretical Paradigms. *Nanomaterials*, 8(6), p.373.
4. Azoidis, I., Cox, S. and Davies, O. (2018). The role of extracellular vesicles in biomineralisation: current perspective and application in regenerative medicine. *Journal of Tissue Engineering*, 9, pp.1-11.
5. Bebelman, M.P., Smit, M.J., Pegtel, D.M. and Baglio, S.R. (2018). Biogenesis and function of extracellular vesicles in cancer. *Pharmacology & therapeutics*, 188, pp.1-11.
6. Bennett, M.H., Stanford, R.E. and Turner, R. (2012). Hyperbaric oxygen therapy for promoting fracture healing and treating fracture non-union. *The Cochrane Library*.
7. Bonucci, E. (1967). Fine structure of early cartilage calcification. *Journal of ultrastructure research*, 20(1-2), pp.33-50.
8. Borosch, S., Dahmen, E., Beckers, C., Stoppe, C., Buhl, E.M., Denecke, B., Goetzenich, A. and Kraemer, S. (2017). Characterization of extracellular vesicles derived from cardiac cells in an in vitro model of preconditioning. *Journal of extracellular vesicles*, 6(1), p.1390391.
9. Borra, R., Lotufo, M., Gagioti, S., Barros, F. and Andrade, P. (2009). A simple method to measure cell viability in proliferation and cytotoxicity assays. *Brazilian Oral Research*, 23(3), pp.255-262.
10. Bruno, S., Porta, S. and Bussolati, B. (2016). Extracellular vesicles in renal tissue damage and regeneration. *European Journal of Pharmacology*, 790, pp.83-91.

11. Centeno, C.J., Schultz, J.R., Cheever, M., Robinson, B., Freeman, M. and Marasco, W. (2010). Safety and complications reporting on the re-implantation of culture-expanded mesenchymal stem cells using autologous platelet lysate technique. *Current stem cell research & therapy*, 5(1), pp.81-93.
12. Chamy, R. and Rosenkranz, F. (2013). Antimicrobial modifications of polymers, in Sedlarik, V., *Biodegradation-Life of Science*, pp.187-204.
13. Chaplin, M. (2018). Gelatin. [online] Water structure and science. Available at: http://www1.lsbu.ac.uk/water/gelatin.html#sou [Accessed 3 Aug. 2019].
14. Chen, B.Y., Sung, C.W.H., Chen, C., Cheng, C.M., Lin, D.P.C. and Hsu, M.Y. (2019). Advances in exosomes technology. *Clinica Chimica Acta*, 493, pp. 14-19.
15. Cheung, L., Sahloul, S., Orozaliev, A. and Song, Y.A. (2018). Rapid Detection and Trapping of Extracellular Vesicles by Electrokinetic Concentration for Liquid Biopsy on Chip. *Micromachines*, 9(6), p.306.
16. Collins, M.N. and Birkinshaw, C. (2013). Hyaluronic acid based scaffolds for tissue engineering—A review. *Carbohydrate polymers*, 92(2), pp.1262-1279.
17. Cooper, I.R. (2015). Introduction to biomaterials and medical device- associated infections, in Barnes, L. and Cooper, I.R. *Biomaterials and medical device-associated infections.* pp. 3-17.
18. Cunnane, E.M., Weinbaum, J.S., O'Brien, F.J. and Vorp, D.A. (2018). Future perspectives on the role of stem cells and extracellular vesicles in vascular tissue regeneration. *Frontiers in cardiovascular medicine*, 5, p.86.
19. Davies, O.G., Cox, S.C., Williams, R.L., Tsaroucha, D., Dorrepaal, R.M., Lewis, M.P. and Grover, L.M. (2017). Annexin-enriched osteoblast-derived vesicles act as an extracellular site of mineral nucleation within developing stem cell cultures. *Scientific reports*, 7(1), p.12639.
20. De Jong, O.G., Van Balkom, B.W., Schiffelers, R.M., Bouten, C.V. and Verhaar, M.C. (2014). Extracellular vesicles: potential roles in regenerative medicine. *Frontiers in immunology*, 5, p.608.
21. De Witte, T.M., Fratila-Apachitei, L.E., Zadpoor, A.A. and Peppas, N.A. (2018). Bone tissue engineering via growth factor delivery: from scaffolds to complex matrices. *Regenerative biomaterials*, 5(4), pp.197-211.

22. Deng, M., G Kumbar, S., W-H Lo, K., D Ulery, B. and T Laurencin, C. (2011). Novel polymer-ceramics for bone repair and regeneration. *Recent Patents on Biomedical Engineering*, 4(3), pp.168-184.
23. Deshmukh, K., Ahamed, M.B., Deshmukh, R.R., Pasha, S.K., Bhagat, P.R. and Chidambaram, K. (2017). Biopolymer composites with high dielectric performance: interface engineering, in *Biopolymer Composites in Electronics*, pp. 27-128.
24. Dong, C. and Lv, Y. (2016). Application of Collagen Scaffold in Tissue Engineering: Recent Advances and New Perspectives. *Polymers*, 8(2), p.42.
25. Drury, J.L. and Mooney, D.J. (2003). Hydrogels for tissue engineering: scaffold design variables and applications. *Biomaterials*, 24(24), pp.4337-4351.
26. Duconseille, A., Astruc, T., Quintana, N., Meersman, F. and Sante-Lhoutellier, V. (2015). Gelatin structure and composition linked to hard capsule dissolution: A review. *Food Hydrocolloids*, 43, pp.360-376.
27. Dujardin, E. and Mann, S. (2002). Bio-inspired materials chemistry. *Advanced Materials*, 14(11), p.775.
28. Fisher, J.N., Peretti, G.M. and Scotti, C. (2016). Stem cells for bone regeneration: from cell-based therapies to decellularised engineered extracellular matrices. *Stem cells international*, 2016, pp.1-15.
29. Goldring, S.R. and Gravallese, E.M. (1999). Mechanisms of bone loss in inflammatory arthritis: diagnosis and therapeutic implications. *Arthritis Research & Therapy*, 2(1), p.33.
30. Goodman, S.B., Yao, Z., Keeney, M. and Yang, F. (2013). The future of biologic coatings for orthopaedic implants. *Biomaterials*, 34(13), pp.3174-3183.
31. Ha, D., Yang, N. and Nadithe, V. (2016). Exosomes as therapeutic drug carriers and delivery vehicles across biological membranes: current perspectives and future challenges. *Acta Pharmaceutica Sinica B*, 6(4), pp.287-296.
32. Hartjes, T.A., Mytnyk, S., Jenster, G.W., van Steijn, V. and van Royen, M.E. (2019). Extracellular Vesicle Quantification and Characterization: Common Methods and Emerging Approaches. *Bioengineering*, 6(1), p.7.

33. Hoque, M.E., Nuge, T., Yeow, T.K., Nordin, N. and Prasad, R.G.S.V. (2015). Gelatin based scaffolds for tissue engineering-a review. *Polymers Research Journal*, 9(1), p.15.
34. Hu, G., Drescher, K.M. and Chen, X. (2012). Exosomal miRNAs: biological properties and therapeutic potential. *Frontiers in genetics*, 3, p.56.
35. Jahangir, A.A., Nunley, R.M., Mehta, S. and Sharan, A. (2008). Bone-graft substitutes in orthopaedic surgery. *AAos now*, 2(1), pp.35-37.
36. Jayakumar, P. and Di Silvio, L. (2010). Osteoblasts in bone tissue engineering. *Proceedings of the Institution of Mechanical Engineers, Part H: Journal of Engineering in Medicine*, 224(12), pp.1415-1440.
37. Khedmat, S., Momen-Heravi, F. and Pishvaei, M. (2013). A comparison of viscoelastic properties of three root canal sealers. *Journal of dentistry (Tehran, Iran)*, 10(2), p.147.
38. Konoshenko, M.Y., Lekchnov, E.A., Vlassov, A.V. and Laktionov, P.P. (2018). Isolation of extracellular vesicles: general methodologies and latest trends. *BioMed research international*, 2018, pp.1-27.
39. Kooijmans, S.A., Vader, P., van Dommelen, S.M., van Solinge, W.W. and Schiffelers, R.M. (2012). Exosome mimetics: a novel class of drug delivery systems. *Int J Nanomedicine*, 7(1525), p.e41.
40. Kowalczewski, C.J. and Saul, J.M. (2018). Biomaterials for the Delivery of Growth Factors and Other Therapeutic Agents in Tissue Engineering Approaches to Bone Regeneration. *Frontiers in pharmacology*, 9, pp.1-15
41. Kretlow, J.D., Klouda, L. and Mikos, A.G. (2007). Injectable matrices and scaffolds for drug delivery in tissue engineering. *Advanced drug delivery reviews*, 59(4-5), pp.263-273.
42. Kuntsche, J., Horst, J.C. and Bunjes, H. (2011). Cryogenic transmission electron microscopy (cryo-TEM) for studying the morphology of colloidal drug delivery systems. *International journal of pharmaceutics*, 417(1-2), pp.120-137.
43. Lai, R.C., Chen, T.S. and Lim, S.K. (2011). Mesenchymal stem cell exosome: a novel stem cell-based therapy for cardiovascular disease. *Regenerative medicine*, 6(4), pp.481-492.

44. Lai, R.C., Yeo, R.W.Y. and Lim, S.K. (2015). Mesenchymal stem cell exosomes. In *Seminars in Cell & Developmental Biology*, 40, pp.82-88.
45. Lamichhane, T.N., Sokic, S., Schardt, J.S., Raiker, R.S., Lin, J.W. and Jay, S.M. (2014). Emerging roles for extracellular vesicles in tissue engineering and regenerative medicine. *Tissue Engineering Part B: Reviews*, 21(1), pp.45-54.
46. Lanza, R., Langer, R. and Vacanti, J. (2014). *Principles of tissue engineering*. London: Elsevier Academic Press.
47. Lee, K.Y. and Mooney, D.J. (2012). Alginate: properties and biomedical applications. *Progress in polymer science*, *37*(1), pp.106-126.
48. Lee, Y., EL Andaloussi, S. and Wood, M. (2012) Exosomes and microvesicles: extracellular. vesicles for genetic information.transfer and gene therapy. *Human Molecular Genetics*, 21(R1), pp.R125-R134.
49. Li, P., Kaslan, M., Lee, S.H., Yao, J. and Gao, Z. (2017). Progress in exosome isolation techniques. *Theranostics*, *7*(3), p.789.
50. Livshits, M.A., Khomyakova, E., Evtushenko, E.G., Lazarev, V.N., Kulemin, N.A., Semina, S.E., Generozov, E.V. and Govorun, V.M. (2015). Isolation of exosomes by differential centrifugation: theoretical analysis of a commonly used protocol. *Scientific reports*, 5(1), p.17319.
51. Loz Lu, K., Li, H.Y., Yang, K., Wu, J.L., Cai, X.W., Zhou, Y. and Li, C.Q. (2017). Exosomes as potential alternatives to stem cell therapy for intervertebral disc degeneration: in-vitro study on exosomes in interaction of nucleus pulposus cells and bone marrow mesenchymal stem cells. *Stem cell research & therapy*, 8(1), p.108.
52. Lozano-Ramos, I., Bancu, I., Oliveira-Tercero, A., Armengol, M.P., Menezes-Neto, A., Portillo, H.A.D., Lauzurica-Valdemoros, R. and Borràs, F.E. (2015). Size-exclusion chromatography-based enrichment of extracellular vesicles from urine samples. *Journal of extracellular vesicles*, 4(1), p.27369.
53. Magnani, A., Lamponi, S., Rappuoli, R. and Barbucci, R. (1998). Sulphated hyaluronic acids: a chemical and biological characterisation. *Polymer international*, 46(3), pp.225-240.

54. Malvern Panalytical. (2019). Nanoparticle Tracking Analysis (NTA). [online] Available at: https://www.malvernpanalytical.com/en/products/technology/nanoparticle-tracking-analysis [Accessed 16 Mar. 2019].
55. Malvern Panalytical. (2019). Dynamic Light Scattering (DLS). [online] Available at: https://www.malvernpanalytical.com/en/products/technology/light-scattering/dynamic-light-scattering [Accessed 16 Mar. 2019].
56. Mao, A. and Mooney, D. (2015). Regenerative medicine: Current therapies and future directions. *Proceedings of the National Academy of Sciences*, 112(47), pp.14452-14459.
57. Martins, M., Ribeiro, D., Martins, A., Reis, R.L. and Neves, N.M. (2016). Extracellular vesicles derived from osteogenically induced human bone marrow mesenchymal stem cells can modulate lineage commitment. *Stem cell reports*, 6(3), pp.284-291.
58. Matassi, F., Botti, A., Sirleo, L., Carulli, C. and Innocenti, M. (2013). Porous metal for orthopedics implants. *Clinical Cases in Mineral and Bone Metabolism*, 10(2), p.111.
59. Matassi, F., Nistri, L., Paez, D.C. and Innocenti, M. (2011). New biomaterials for bone regeneration. *Clinical cases in mineral and bone metabolism*, 8(1), pp.21-24.
60. Mathew, G. and Hanson, B.P. (2009). Global burden of trauma: need for effective fracture therapies. *Indian journal of orthopaedics*, 43(2), p.111.
61. Mendes, P.M., Fernandez-Trillo, F., Grover, L., Stephenson-Brown, A. and Harrison, P. (2016). Vesicles and their multiple facets: underpinning biological and synthetic progress. *Angewandte Chemie International Edition*.
62. Meyers, M.A., Chen, P.Y., Lin, A.Y.M. and Seki, Y. (2008). Biological materials: structure and mechanical properties. *Progress in Materials Science*, 53(1), pp.1-206.

63. Mol, E.A., Goumans, M.J., Doevendans, P.A., Sluijter, J.P. and Vader, P. (2017). Higher functionality of extracellular vesicles isolated using size-exclusion chromatography compared to ultracentrifugation. *Nanomedicine: Nanotechnology, Biology and Medicine*, 13(6), pp.2061-2065.
64. Momen-Heravi, F., Balaj, L., Alian, S., Mantel, P.Y., Halleck, A.E., Trachtenberg, A.J., Soria, C.E., Oquin, S., Bonebreak, C.M., Saracoglu, E. and Skog, J. (2013). Current methods for the isolation of extracellular vesicles. *Biological chemistry*, 394(10), pp.1253-1262.
65. Momen-Heravi, F., Balaj, L., Alian, S., Tigges, J., Toxavidis, V., Ericsson, M., Distel, R.J., Ivanov, A.R., Skog, J. and Kuo, W.P. (2012). Alternative methods for characterization of extracellular vesicles. *Frontiers in physiology*, 3, p.354.
66. Morhayim, J., Rudjito, R., van Leeuwen, J.P. and van Driel, M. (2016). Paracrine signaling by extracellular vesicles via osteoblasts. *Current molecular biology reports*, 2(1), pp.48-55.
67. Morhayim, J., Van De Peppel, J., Braakman, E., Rombouts, E.W., Ter Borg, M.N., Dudakovic, A., Chiba, H., Van Der Eerden, B.C., Raaijmakers, M.H., Van Wijnen, A.J. and Cornelissen, J.J. (2016). Osteoblasts secrete miRNA-containing extracellular vesicles that enhance expansion of human umbilical cord blood cells. *Scientific reports*, 6, p.32034.
68. Muzzarelli, R.A. (2011). Chitosan composites with inorganics, morphogenetic proteins and stem cells, for bone regeneration. *Carbohydrate Polymers*, 83(4), pp.1433-1445.
69. Nandi, S.K., Roy, S., Mukherjee, P., Kundu, B., De, D.K. and Basu, D. (2010). Orthopaedic applications of bone graft & graft substitutes: a review. *Indian J Med Res*, 132(1), pp.15-30.
70. Navarro, M., Michiardi, A., Castano, O. and Planell, J.A. (2008). Biomaterials in orthopaedics. *Journal of the Royal Society Interface*, 5(27), pp.1137-1158.
71. Nikravesh, N., Davies, O.G., Azoidis, I., Moakes, R.J., Marani, L., Turner, M., Kearney, C.J., Eisenstein, N.M., Grover, L.M. and Cox, S.C. (2019). Physical Structuring of Injectable Polymeric Systems to Controllably Deliver Nanosized Extracellular Vesicles. *Advanced healthcare materials*, p.1801604.

72. Nitta, Y. and Nishinari, K. (2005). Gelation and gel properties of polysaccharides gellan gum and tamarind xyloglucan. *J Biol Macromol*, 5(3), pp.47-52.
73. Niu, Z., Pang, R.T., Liu, W., Li, Q., Cheng, R. and Yeung, W.S. (2017). Polymer-based precipitation preserves biological activities of extracellular vesicles from an endometrial cell line. *PloS one*, 12(10), p.e0186534.
74. Ohi, M., Li, Y., Cheng, Y. and Walz, T. (2004). Negative staining and image classification—powerful tools in modern electron microscopy. *Biological procedures online*, 6(1), p.23.
75. Oliveira, J.T., Martins, L., Picciochi, R., Malafaya, P.B., Sousa, R.A., Neves, N.M., Mano, J.F. and Reis, R.L. (2010). Gellan gum: a new biomaterial for cartilage tissue engineering applications. *Journal of Biomedical Materials Research Part A: An Official Journal of The Society for Biomaterials, The Japanese Society for Biomaterials, and The Australian Society for Biomaterials and the Korean Society for Biomaterials*, 93(3), pp.852-863.
76. Ong, S.G. and Wu, J.C. (2015). Exosomes as potential alternatives to stem cell therapy in mediating cardiac regeneration, *Circulation Research*, 117(1), pp.7-9.
77. Osugi, M., Katagiri, W., Yoshimi, R., Inukai, T., Hibi, H. and Ueda, M. (2012). Conditioned media from mesenchymal stem cells enhanced bone regeneration in rat calvarial bone defects. *Tissue engineering part A*, *18*(13-14), pp.1479-1489.
78. Palmieri, V., Lucchetti, D., Gatto, I., Maiorana, A., Marcantoni, M., Maulucci, G., Papi, M., Pola, R., De Spirito, M. and Sgambato, A. (2014). Dynamic light scattering for the characterization and counting of extracellular vesicles: a powerful noninvasive tool. *Journal of nanoparticle research*, 16(9), p.2583.
79. Parida, P., Behera, A. and Mishra, S.C. (2012). Classification of Biomaterials used in Medicine. *International Journal of Advances in Applied Sciences*, 1(3), pp.31-35.
80. Particle sizing systems, PSS. (2018). Dynamic Light Scattering (DLS). [online] Available at: http://pssnicomp.com/glossary/dynamic-light-scattering-dls/ [Accessed 8 Feb. 2019].

81. Perez-Pujol, S., Marker, P. and Key, N. (2007). Platelet microparticles are heterogeneous and highly dependent on the activation mechanism: Studies using a new digital flow cytometer. *Cytometry Part A*, 71(1), pp.38-45.
82. Perez, R.A., Seo, S.J., Won, J.E., Lee, E.J., Jang, J.H., Knowles, J.C. and Kim, H.W. (2015). Therapeutically relevant aspects in bone repair and regeneration. *Materials Today*, 18(10), pp.573-589.
83. Polykandriotis, E., Popescu, L.M. and Horch, R.E. (2010). Regenerative medicine: then and now–an update of recent history into future possibilities. *Journal of cellular and molecular medicine*, 14(10), pp.2350-2358.
84. Prasad, B. and Mandal, B. (2018). Moisture responsive and CO2 selective biopolymer membrane containing silk fibroin as a green carrier for facilitated transport of CO2. *Journal of Membrane Science*, 550, pp.416-426.
85. Pulat, M. and Akalin, G.O. (2013). Preparation and characterization of gelatin hydrogel support for immobilization of Candida Rugosa lipase. *Artificial cells, nanomedicine, and biotechnology*, 41(3), pp.145-151.
86. Qi, Y., Wang, H., Wei, K., Yang, Y., Zheng, R.Y., Kim, I. and Zhang, K.Q. (2017). A review of structure construction of silk fibroin biomaterials from single structures to multi-level structures. *International journal of molecular sciences*, 18(3), p.237.
87. Qin, Y., Sun, R., Wu, C., Wang, L. and Zhang, C. (2016). Exosome: a novel approach to stimulate bone regeneration through regulation of osteogenesis and angiogenesis. *International journal of molecular sciences*, 17(5), p.712.
88. Qin, Y., Wang, L., Gao, Z., Chen, G. and Zhang, C. (2016). Bone marrow stromal/stem cell-derived extracellular vesicles regulate osteoblast activity and differentiation in vitro and promote bone regeneration in vivo. *Scientific reports*, 6, p.21961.
89. Radhakrishnan, J., Subramanian, A., Krishnan, U.M. and Sethuraman, S. (2016). Injectable and 3D bioprinted polysaccharide hydrogels: from cartilage to osteochondral tissue engineering. *Biomacromolecules*, 18(1), pp.1-26.

90. Raimondo, F., Morosi, L., Chinello, C., Magni, F. and Pitto, M. (2011). Advances in membranous vesicle and exosome proteomics improving biological understanding and biomarker discovery. *Proteomics*, 11(4), pp.709-720.
91. Rampersad, S. (2012). Multiple Applications of Alamar Blue as an Indicator of Metabolic Function and Cellular Health in Cell Viability Bioassays. *Sensors*, 12(9), pp.12347-12360.
92. Raposo, G. and Stoorvogel, W. (2013). Extracellular vesicles: exosomes, microvesicles, and friends. *J Cell Biol*, 200(4), pp.373-383.
93. Raposo, G., Nijman, H.W., Stoorvogel, W., Liejendekker, R., Harding, C.V., Melief, C.J. and Geuze, H.J. (1996). B lymphocytes secrete antigen-presenting vesicles. *Journal of Experimental Medicine*, 183(3), pp.1161-1172.
94. Ratajczak, M.Z., Kucia, M., Jadczyk, T., Greco, N.J., Wojakowski, W., Tendera, M. and Ratajczak, J. (2012). Pivotal role of paracrine effects in stem cell therapies in regenerative medicine: can we translate stem cell-secreted paracrine factors and microvesicles into better therapeutic strategies?. *Leukemia*, 26(6), p.1166.
95. Rayner, K.J. and Hennessy, E.J. (2013). Extracellular communication via microRNA: lipid particles have a new message. *Journal of lipid research*, 54(5), pp.1174-1181.
96. Reisman, M. and Adams, K.T. (2014). Stem cell therapy: A look at current research, regulations, and remaining hurdles. *Pharmacy and Therapeutics*, 39(12), p.846.
97. Robert, S., Poncelet, P., Lacroix, R., Arnaud, L., Giraudo, L., Hauchard, A., Sampol, J. and Dignat-George, F. (2009). Standardization of platelet-derived microparticle counting using calibrated beads and a Cytomics FC500 routine flow cytometer: a first step towards multicenter studies?. *Journal of Thrombosis and Haemostasis*, 7(1), pp.190-197.
98. Roberts, T.T. and Rosenbaum, A.J. (2012). Bone grafts, bone substitutes and orthobiologics: the bridge between basic science and clinical advancements in fracture healing. *Organogenesis*, 8(4), pp.114-124.
99. Ronquist, G. and Brody, I. (1985). The prostasome: its secretion and function in man. *Biochimica et biophysica acta*, 822(2), pp.203-218.

100. Rupert, D.L., Claudio, V., Lässer, C. and Bally, M. (2017). Methods for the physical characterization and quantification of extracellular vesicles in biological samples. *Biochimica et Biophysica Acta (BBA)-General Subjects*, 1861(1), pp.3164-3179.

101. Schlötzer-Schrehardt, U., Polisetti, N., Menzel-Severing, J. and Kruse, F.E. (2013). Tissue Engineering for Reconstruction of the Corneal Epithelium. In *Ocular Surface Disease: Cornea, Conjunctiva and Tear Film*, pp. 347-360.

102. Serrano-Pertierra, E., Oliveira-Rodríguez, M., Rivas, M., Oliva, P., Villafani, J., Navarro, A., Blanco-López, M.C. and Cernuda-Morollón, E. (2019). Characterization of Plasma-Derived Extracellular Vesicles Isolated by Different Methods: A Comparison Study. *Bioengineering*, 6(1), p.8.

103. Sheikh, Z., Najeeb, S., Khurshid, Z., Verma, V., Rashid, H. and Glogauer, M. (2015). Biodegradable materials for bone repair and tissue engineering applications. *Materials*, 8(9), pp.5744-5794.

104. Stevens, M.M. (2008). Biomaterials for bone tissue engineering. *Materials today*, 11(5), pp.18-25.

105. Sworn, G. (2009). Gellan gum. In Phillips, G. and Williams, P. *Handbook of Hydrocolloids (Second Edition).* pp. 204-227.

106. Szatanek, R., Baj-Krzyworzeka, M., Zimoch, J., Lekka, M., Siedlar, M. and Baran, J. (2017). The methods of choice for extracellular vesicles (EVs) characterization. *International journal of molecular sciences*, 18(6), p.1153.

107. Szatanek, R., Baran, J., Siedlar, M. and Baj-Krzyworzeka, M. (2015). Isolation of extracellular vesicles: Determining the correct approach (Review). *International journal of molecular medicine*, 36(1), pp.11-17.

108. Tatischeff, I., Larquet, E., Falcón-Pérez, J.M., Turpin, P.Y. and Kruglik, S.G. (2012). Fast characterisation of cell-derived extracellular vesicles by nanoparticles tracking analysis, cryo-electron microscopy, and Raman tweezers microspectroscopy. *Journal of extracellular vesicles*, 1(1), p.19179.

109. Tauro, B.J., Greening, D.W., Mathias, R.A., Ji, H., Mathivanan, S., Scott, A.M. and Simpson, R.J. (2012). Comparison of ultracentrifugation, density gradient separation, and immunoaffinity capture methods for isolating human colon cancer cell line LIM1863-derived exosomes. *Methods*, *56*(2), pp.293-304.

110. Théry, C., Amigorena, S., Raposo, G. and Clayton, A. (2006). Isolation and characterization of exosomes from cell culture supernatants and biological fluids. *Current protocols in cell biology*, 30(1), pp.3-22.

111. Théry, C., Witwer, K.W., Aikawa, E., Alcaraz, M.J., Anderson, J.D., Andriantsitohaina, R., Antoniou, A., Arab, T., Archer, F., Atkin-Smith, G.K. and Ayre, D.C. (2018). Minimal information for studies of extracellular vesicles 2018 (MISEV2018): a position statement of the International Society for Extracellular Vesicles and update of the MISEV2014 guidelines. *Journal of Extracellular Vesicles*, 7(1), p.1535750.

112. Tozzi, G., De Mori, A., Oliveira, A. and Roldo, M. (2016). Composite hydrogels for bone regeneration. *Materials*, 9(4), p.267.

113. Tsou, Y.H., Khoneisser, J., Huang, P.C. and Xu, X. (2016). Hydrogel as a bioactive material to regulate stem cell fate. *Bioactive Materials*, 1(1), pp.39-55.

114. Van der Pol, E., Coumans, F.A.W., Grootemaat, A.E., Gardiner, C., Sargent, I.L., Harrison, P., Sturk, A., Van Leeuwen, T.G. and Nieuwland, R. (2014). Particle size distribution of exosomes and microvesicles determined by transmission electron microscopy, flow cytometry, nanoparticle tracking analysis, and resistive pulse sensing. *Journal of Thrombosis and Haemostasis*, 12(7), pp.1182-1192.

115. Van Der Pol, E., Hoekstra, A.G., Sturk, A., Otto, C.V., Van Leeuwen, T.G. and Nieuwland, R. (2010). Optical and non-optical methods for detection and characterization of microparticles and exosomes. *Journal of Thrombosis and Haemostasis*, 8(12), pp.2596-2607.

116. van Dommelen, S.M., Vader, P., Lakhal, S., Kooijmans, S.A.A., van Solinge, W.W., Wood, M.J. and Schiffelers, R.M. (2012). Microvesicles and exosomes: opportunities for cell-derived membrane vesicles in drug delivery. *Journal of Controlled Release*, 161(2), pp.635-644.

117. Venkatesan, J. and Kim, S.K. (2010). Chitosan composites for bone tissue engineering—an overview. Marine drugs, 8(8), pp.2252-2266.

118. Venkatesan, J., Bhatnagar, I., Manivasagan, P., Kang, K.H. and Kim, S.K. (2015). Alginate composites for bone tissue engineering: a review. *International journal of biological macromolecules*, 72, pp.269-281.

119. Vestad, B., Llorente, A., Neurauter, A., Phuyal, S., Kierulf, B., Kierulf, P., Skotland, T., Sandvig, K., Haug, K.B.F. and Øvstebø, R. (2017). Size and concentration analyses of extracellular vesicles by nanoparticle tracking analysis: a variation study. *Journal of extracellular vesicles*, 6(1), p.1344087.

120. Vicencio, J.M., Yellon, D.M., Sivaraman, V., Das, D., Boi-Doku, C., Arjun, S., Zheng, Y., Riquelme, J.A., Kearney, J., Sharma, V. and Multhoff, G. (2015). Plasma exosomes protect the myocardium from ischemia-reperfusion injury. *Journal of the American College of Cardiology*, 65(15), pp.1525-1536.

121. Vishnubhatla, I., Corteling, R., Stevanato, L., Hicks, C. and Sinden, J. (2014). The development of stem cell-derived exosomes as a cell-free regenerative medicine. *Journal of Circulating Biomarkers*, 3(Godište 2014), pp.3-2.

122. Vrijsen, K.R., Sluijter, J.P.G., Schuchardt, M.W.L., Van Balkom, B.W.M., Noort, W.A., Chamuleau, S.A.J. and Doevendans, P.A.F.M. (2010). Cardiomyocyte progenitor cell-derived exosomes stimulate migration of endothelial cells. *Journal of cellular and molecular medicine*, 14(5), pp.1064-1070.

123. Wang, M., Yuan, Z., Ma, N., Hao, C., Guo, W., Zou, G., Zhang, Y., Chen, M., Gao, S., Peng, J. and Wang, A. (2017). Advances and prospects in stem cells for cartilage regeneration. *Stem cells international*, 2017, pp.1-16.

124. Wang, W. and Yeung, K. (2017). Bone grafts and biomaterials substitutes for bone defect repair: A review. *Bioactive Materials*, 2(4), pp.224-247.

125. Wang, X., Ao, Q., Tian, X., Fan, J., Tong, H., Hou, W. and Bai, S. (2017). Gelatin-based hydrogels for organ 3D bioprinting. *Polymers*, 9(9), p.401.

126. Wang, Z., Wu, H.J., Fine, D., Schmulen, J., Hu, Y., Godin, B., Zhang, J.X. and Liu, X. (2013). Ciliated micropillars for the microfluidic-based isolation of nanoscale lipid vesicles. *Lab on a Chip*, 13(15), pp.2879-2882.

127. Wei, X., Yang, X., Han, Z.P., Qu, F.F., Shao, L. and Shi, Y.F. (2013). Mesenchymal stem cells: a new trend for cell therapy. *Acta Pharmacologica Sinica*, 34(6), p.747.

128. Williams, D.F. (1999). Dictionary of biomaterials. *Liverpool, Liverpool University Prees*, p.42.

129. Williams, D.F. (2008) On the mechanisms of biocompatibility. *Biomaterials*, 29(20), pp.2941-2953.

130. Willms, E., Cabañas, C., Mäger, I., Wood, M. and Vader, P. (2018). Extracellular vesicle heterogeneity: subpopulations, isolation techniques and diverse functions in cancer progression. *Frontiers in immunology*, 9, p.738.

131. Willms, E., Johansson, H.J., Mäger, I., Lee, Y., Blomberg, K.E.M., Sadik, M., Alaarg, A., Smith, C.E., Lehtiö, J., Andaloussi, S.E. and Wood, M.J. (2016). Cells release subpopulations of exosomes with distinct molecular and biological properties. *Scientific reports*, 6, p.22519.

132. Winkler, T., Sass, F.A., Duda, G.N. and Schmidt-Bleek, K. (2018). A review of biomaterials in bone defect healing, remaining shortcomings and future opportunities for bone tissue engineering: The unsolved challenge. *Bone & Joint Research*, 7(3), pp.232-243.

133. Witwer, K.W., Buzas, E.I., Bemis, L.T., Bora, A., Lässer, C., Lötvall, J., Nolte, E.N., Piper, M.G., Sivaraman, S., Skog, J. and Théry, C. (2013). Standardization of sample collection, isolation and analysis methods in extracellular vesicle research. *Journal of extracellular vesicles*, 2(1), p.20360.

134. Wolf, P. (1967). The nature and significance of platelet products in human plasma. *British journal of haematology*, 13(3), pp.269-288.

135. Wu, M., Ouyang, Y., Wang, Z., Zhang, R., Huang, P.H., Chen, C., Li, H., Li, P., Quinn, D., Dao, M. and Suresh, S. (2017). Isolation of exosomes from whole blood by integrating acoustics and microfluidics. *Proceedings of the National Academy of Sciences*, 114(40), pp.10584-10589.

136. Xiao, Z., Camalier, C.E., Nagashima, K., Chan, K.C., Lucas, D.A., Cruz, M.J.D.L., Gignac, M., Lockett, S., Issaq, H.J., Veenstra, T.D. and Conrads, T.P. (2007). Analysis of the extracellular matrix vesicle proteome in mineralizing osteoblasts. *Journal of cellular physiology*, 210(2), pp.325-335.

137. Yakimchuk, K. (2015). Exosomes: isolation methods and specific markers. *Materials and Methods*, 5, p.1450.

138. Yáñez-Mó, M., Siljander, P.R.M., Andreu, Z., Bedina Zavec, A., Borràs, F.E., Buzas, E.I., Buzas, K., Casal, E., Cappello, F., Carvalho, J. and Colás, E. (2015). Biological properties of extracellular vesicles and their physiological functions. *Journal of extracellular vesicles*, 4(1), p.27066.

139. Yeo, R.W.Y., Lai, R.C., Tan, K.H. and Lim, S.K. (2013). Exosome: a novel and safer therapeutic refinement of mesenchymal stem cell. *Exosomes and Microvesicles*, 1, p.7.

140. Yuan, A., Farber, E.L., Rapoport, A.L., Tejada, D., Deniskin, R., Akhmedov, N.B. and Farber, D.B. (2009). Transfer of microRNAs by embryonic stem cell microvesicles. *PloS one*, 4(3), p.e4722.

141. Yuana, Y., Koning, R.I., Kuil, M.E., Rensen, P.C., Koster, A.J., Bertina, R.M. and Osanto, S. (2013). Cryo-electron microscopy of extracellular vesicles in fresh plasma. *Journal of extracellular vesicles*, 2(1), p.21494.

142. Yuana, Y., Sturk, A. and Nieuwland, R. (2013). Extracellular vesicles in physiological and pathological conditions. *Blood reviews*, *27*(1), pp.31-39.

143. Zabeo, D., Cvjetkovic, A., Lasser, C., Schorb, M., Lotvall, J. and Hoog, J.L. (2017). Exosomes purified from a single cell type have diverse morphology. *Journal of Extracellular Vesicles*, 6(1), p.1329476.

144. Zaborowski, M.P., Balaj, L., Breakefield, X.O. and Lai, C.P. (2015). Extracellular vesicles: Composition, biological relevance, and methods of study. *Bioscience*, 65(8), pp.783-797.

145. Zhang, B., Myers, D., Wallace, G., Brandt, M. and Choong, P. (2014). Bioactive coatings for orthopaedic implants—recent trends in development of implant coatings. *International Journal of Molecular Sciences*, 15(7), pp.11878-11921.

146. Zhang, N., Wardwell, P. and Bader, R. (2013). Polysaccharide-based micelles for drug delivery. *Pharmaceutics*, 5(2), pp.329-352.

147. Zhou, J., Ghoroghi, S., Benito-Martin, A., Wu, H., Unachukwu, U.J., Einbond, L.S., Guariglia, S., Peinado, H. and Redenti, S. (2016). Characterization of induced pluripotent stem cell microvesicle genesis, morphology and pluripotent content. *Scientific reports*, 6, p.19743.

APPENDICES

Appendix A - Frequency sweep measurement for sample 1

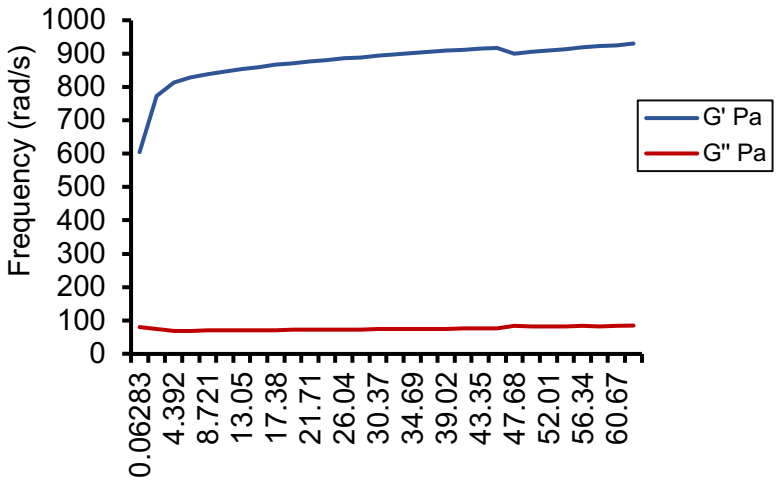

Storage and Loss modulus: G' and G" (Pa)

Appendix B - Frequency sweep measurement for sample 2

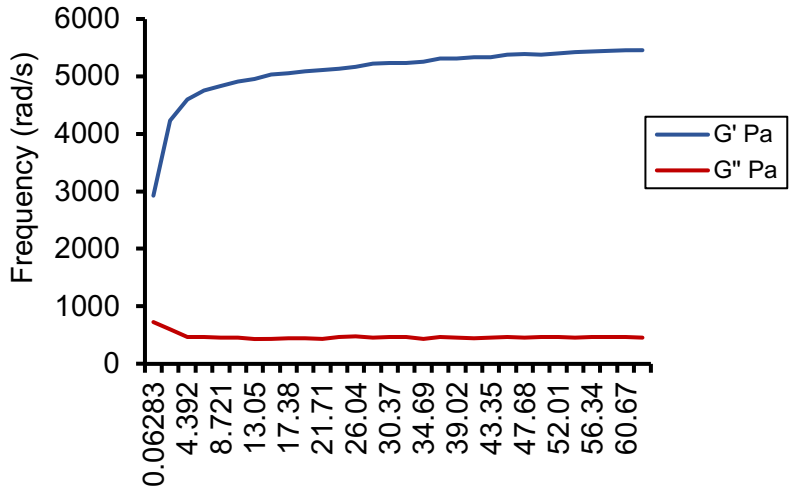

Storage and Loss modulus: G' and G" (Pa)

Appendix C - Frequency sweep measurement for sample 3

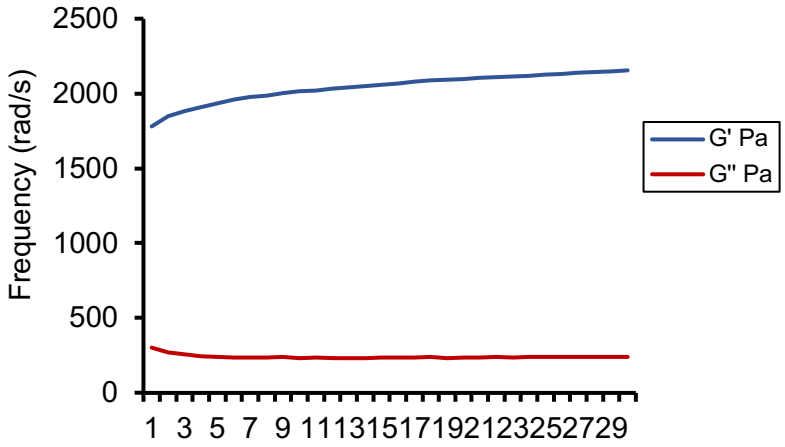

Storage and Loss modulus: G’ and G” (Pa)

Appendix D - Frequency sweep measurement for sample 5

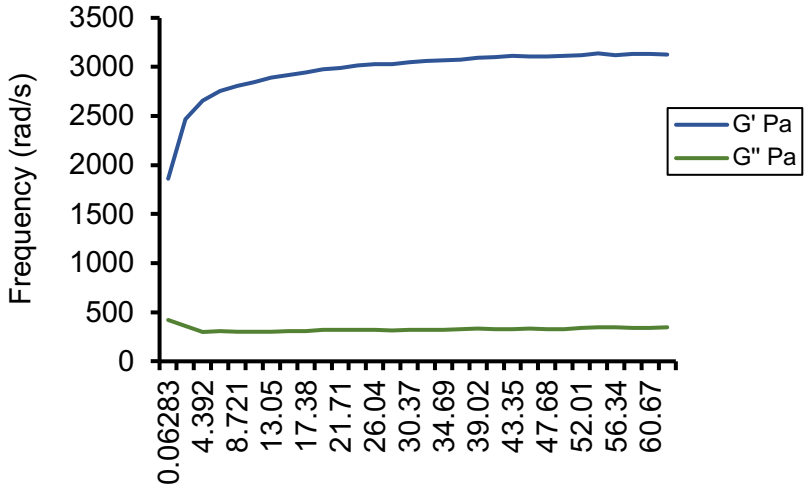

Storage and Loss modulus: G’ and G” (Pa)

Appendix E - Frequency sweep measurement for sample 6

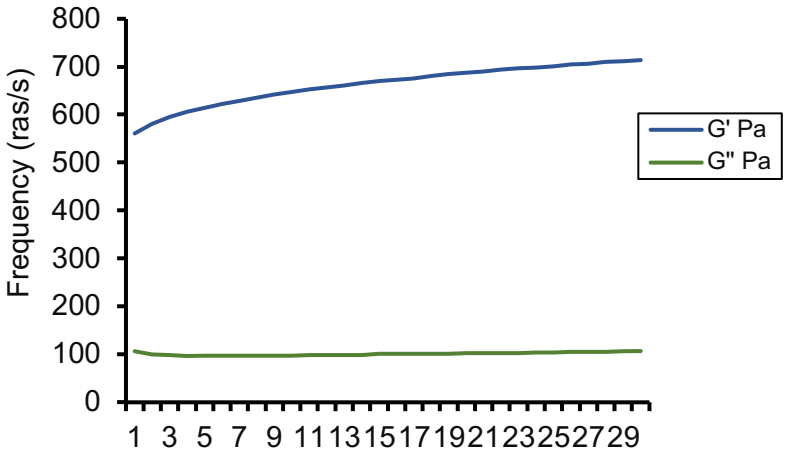

Storage and Loss modulus: G’ and G” (Pa)

Appendix F - Frequency sweep measurement for sample 7

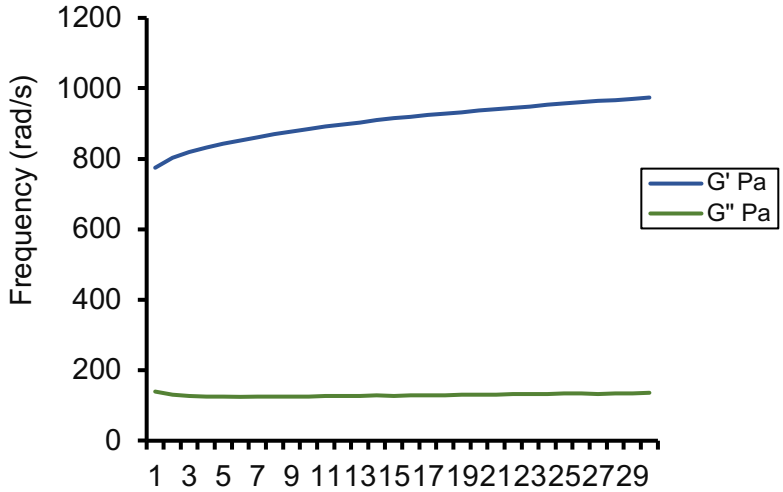

Storage and Loss modulus: G’ and G” (Pa)